ATTACHMENT 1
VALIDATION TEST PLAN (VTP) RESULTS
for the
FEHM Application Version 2.21

Los Alamos National Laboratory

TABLE OF CONTENTS - VTP RESULTS

LIST OF FIGURES

LIST OF TABLES

1.0   OVERVIEW

1.1   SCOPE OF VALIDATION ACTIVITIES

The overall validation effort for the **FEHM** application consists of rigorous and complete testing of the model, whenever possible, against known analytical solutions of the same problem. An alternative approach for more complex test cases for which no analytical solution exists is to benchmark the code against the results of other numerical models. The problems tested are described in detail in the main body of this document (hence forth, referred to as the FEHM VTP).

1.2   DESCRIPTION OF ENVIRONMENT

Verification of **FEHM** was performed on the following platforms: Sun SPARC UNIX (Solaris 7, 8, 9) and PC (Windows 2000 and Linux 2.4.18, 2.4.19). It is anticipated that the code should function on other standard UNIX systems or later versions of the operating systems listed.

A series of test scripts have been developed to automate the verification procedure. They are described in more detail in the APPENDIX: FEHM VALIDATION SCRIPTS of the FEHM VTP.

1.3   ADDITIONAL VALIDATION ISSUES

This validation effort attempts to test each of the major sub-models in FEHM against an analytical solution or the results of another flow and transport code. Heat transfer, isothermal fluid flow, coupled heat and mass transfer, and solute transport test cases are included. For any of these individual runs, there are numerous "minor" options available, such as input-output options, the ability to restart calculations, and the ability to set properties on a node-by-node or zone-by-zone basis, that are not included in this report. These options have been extensively debugged, tested, and documented, but in the interest of space and time limitations, are outside the scope of the formal testing effort.

Model validation is another area that is outside the scope of this report. A large field testing effort is being undertaken in the Yucca Mountain Project to test the validity of the conceptual models and build confidence in them. However, these studies are scientific studies that are not covered in this document, which focuses only on code verification, the process of determining that the physical models have been properly implemented in the computer code.

2.0   DISCUSSION OF TEST RESULTS

The problems discussed below correspond directly to those described in Section 2.0 of the FEHM VTP. The numerical comparisons of results are generated using the formulae given in Section 1.3 of the FEHM VTP. Although all tests are run for each version and specified platform, values provided in the results tables contained in this attachment are not necessarily updated for each revision of the code and documentation. They are provided as being representative of the expected results. Minor variations are expected to occur as the code evolves and when executing the problems on the different platforms. Acceptance of the test results should be based on the criteria specified in the main body of the FEHM VTP, not on the values presented here.

2.1   Testing of Thermodynamic Functions

2.1.1   Enthalpy

These tests verify that the FEHM enthalpy functions provide accurate values of enthalpy as illustrated in Figure 1. The results, compared numerically to the values used to generate the enthalpy functions (found in files thermo.steam_table_data.liq and thermo.steam_table_data.vap), are given in Table I. The maximum absolute error for liquid enthalpy was less than 0.003 MJ/kg, and the percent error was less than 0.2%. The maximum absolute error for vapor enthalpy was 0.0001 MJ/kg, and the percent error was less than 0.004%. These results meet the acceptance criteria for this test suite as developed in the FEHM VTP.

A spot check of liquid enthalpies calculated for temperatures below 15 °C, indicates that errors will exceed the acceptance criteria when pressures are below 8 MPa, and temperatures are below 3 °C. For a temperature of 0.5°C, at a pressure of 0.001 MPa the error in enthalpy was 0.00027 MJ/kg, 13.2 % of the steam table value, while it was 0.00021 MJ/kg, 2.5 % of the steam table value for a temperature of 2 °C. Errors for vapor enthalpies calculated for temperatures below 15 °C, still meet the acceptance criteria.

Table I. Results of Thermodynamic Function Tests			
V&V Test	Maximum Error	Maximum % Error	RMS Error
Enthalpy			
Liquid	2.100e-03	0.1319	1.732e-05
Vapor	9.000e-05	3.125e-03	3.130e-06
Density			
Liquid	1.5220	0.2482	2.018e-05
Vapor	2.550e-02	5.794e-02	6.295e-05
Compressibility			
Liquid	2.160e-03	16.0000	5.182e-03
Vapor	1.2870	0.1297	4.074e-04
Viscosity			
Liquid	3.224e-06	0.5244	9.222e-05
Vapor	3.650e-08	0.1601	1.687e-04
Saturation Pressure and Temperature			
Pressure	2.575e-02	0.3000	4.687e-04
Temperature	1.1000	0.4000	5.943e-04

2.1.2   Density

These tests verify that the FEHM density functions provide accurate values of density as illustrated in Figure 2. The results, compared numerically to the values used to generate the density functions (found in files thermo.steam_table_data.liq and thermo.steam_table_data.vap), are given in Table I. The maximum absolute error for liquid density was less than 1.6 m^3/kg, and the percent error was less than 0.3%. The maximum
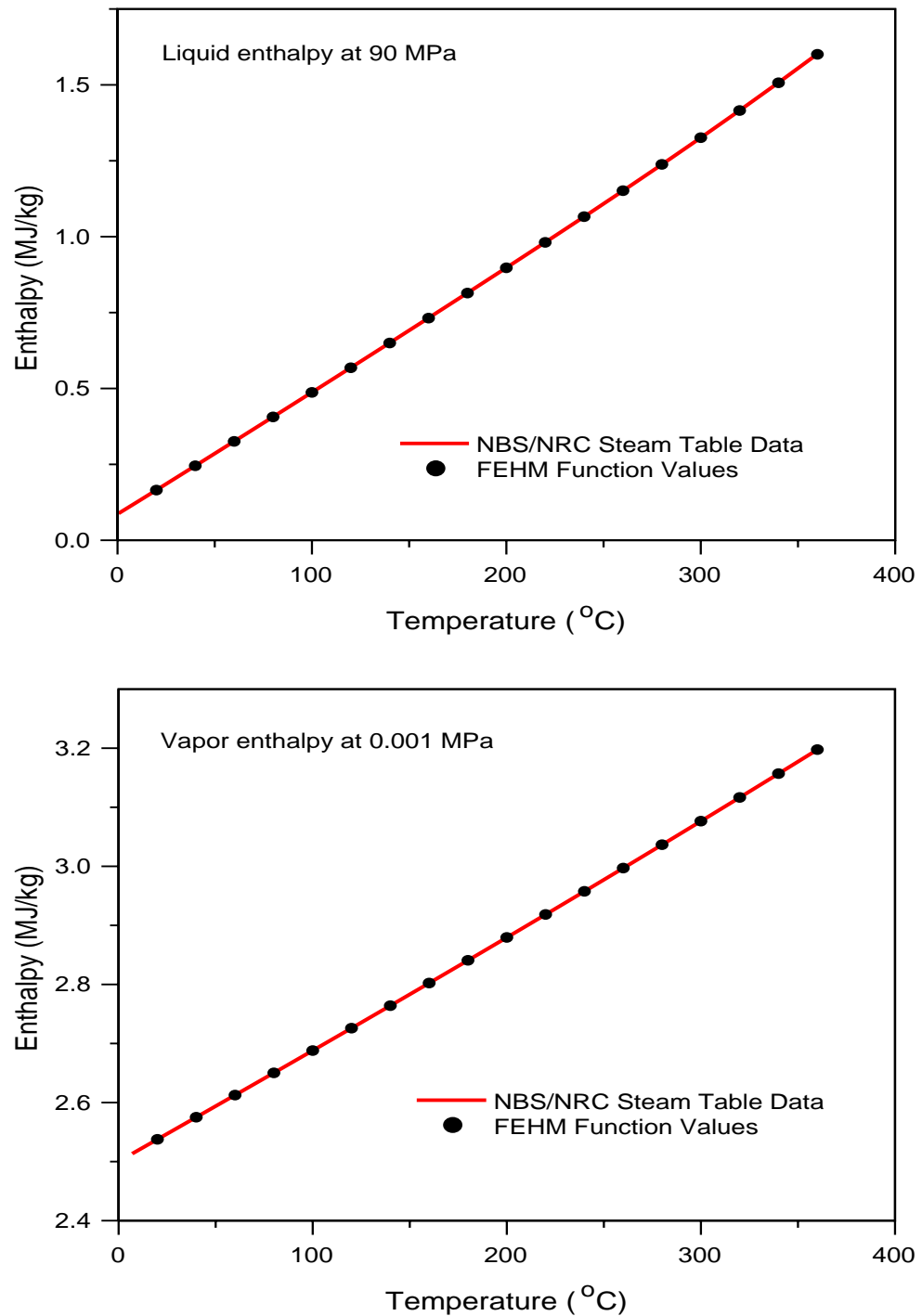
Figure 1. Comparison of FEHM enthalpies to National Bureau of Standards Steam Table Data.

absolute error for vapor density was 0.026 m³/kg, and the percent error was less than 0.06%. These results meet the acceptance criteria for this test suite as developed in the FEHM VTP. A spot check of densities calculated for temperatures below 15 °C, indicates that errors (for both liquid and vapor density) still meet the acceptance criteria.
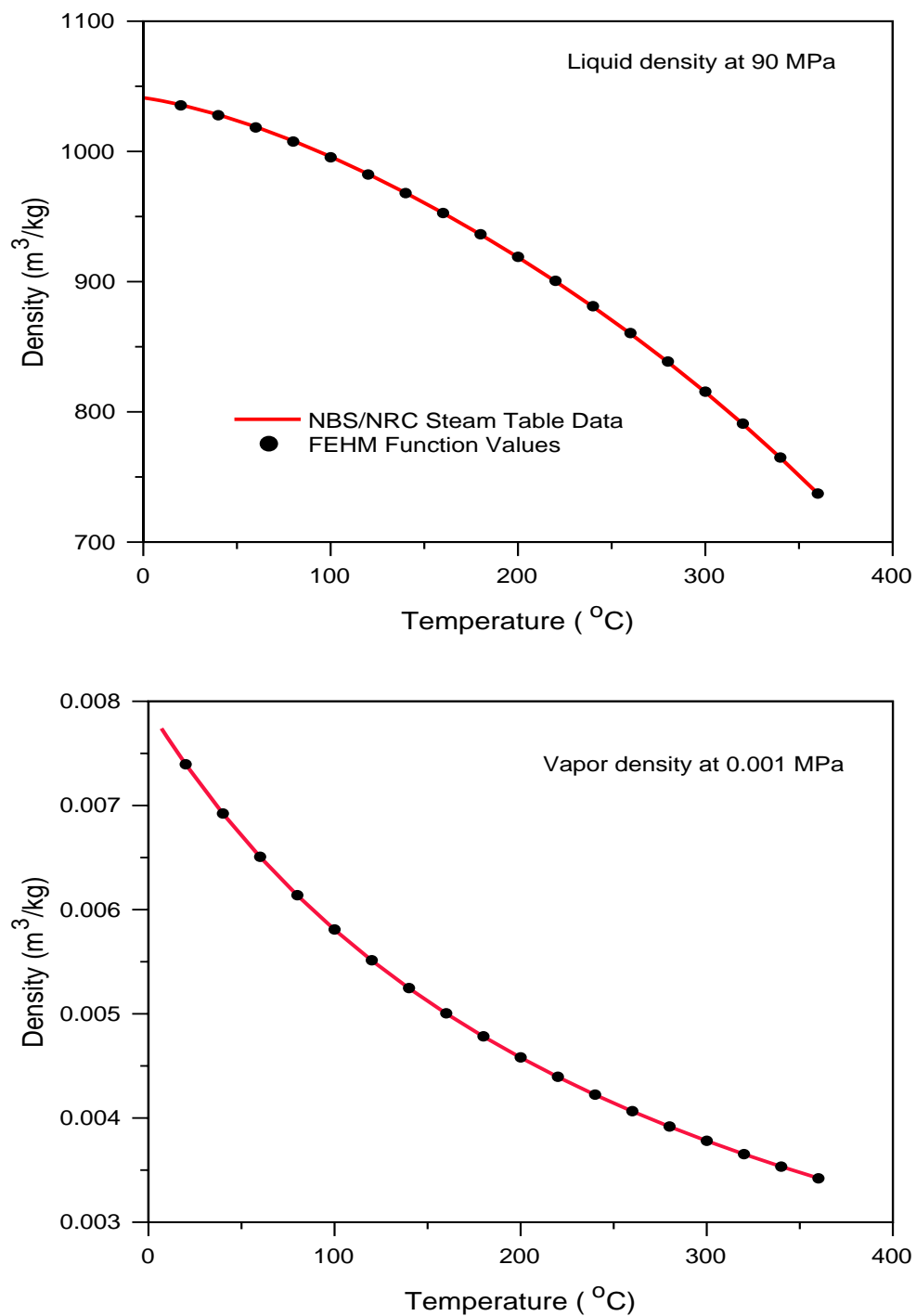
Figure 2.   Comparison of FEHM densities to National Bureau of Standards Steam Table Data.

2.1.3   Compressibility (Derivative of Density with Respect to Pressure)

These tests verify that the FEHM compressibility functions provide accurate values of compressibility as illustrated in Figure 3. The results, compared numerically to the values used to generate the compressibility functions (found in files thermo.compress_data.liq and

thermo.compress_data.vap), are given in Table I. The maximum absolute error for liquid compressibility was less than 0.0022 MPa^{-1}, the percent error was 16%, and the RMS error was less than 0.006. The maximum absolute error for vapor compressibility was 1.3 MPa^{-1}, the percent error was less than 0.2%, and the RMS error was less than 0.0005. These results meet the acceptance criteria for this test suite as developed in the FEHM VTP. Although the liquid compressibility had a maximum error greater than 10%, the RMS error was within acceptable limits. It is important to note that this calculated value of liquid compressibility is never used in the governing equations. This is shown best in the accurate solution of the fully saturated Theis problem (see Section 2.5), which would be most sensitive to liquid compressibility deviations.

A spot check of liquid compressibilities calculated for temperatures below 15 °C, indicates that though percent errors are large (i.e., for a temperature of 0.5°C, at a pressure of 0.001 MPA, the error in compressibility was 0.00016 MPa, 32.3% of the steam table value), values still meet the RMS error acceptance criteria.
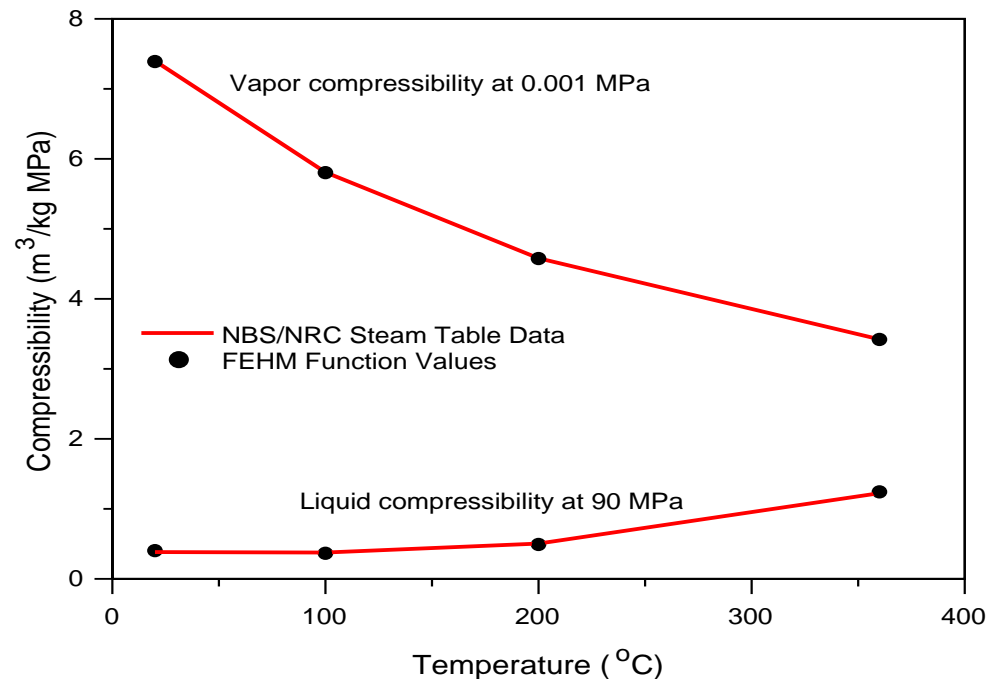
Figure 3.   Comparison of FEHM compressibilities to National Bureau of Standards Steam Table Data.

2.1.4 Viscosity

These tests verify that the FEHM viscosity functions provide accurate values of viscosity as illustrated in Figure 4. The results, compared numerically to the values used to generate the enthalpy functions (found in files thermo.steam_table_data.liq and thermo.steam_table_data.vap), are given in Table I. The maximum absolute error for liquid viscosity was 3.2e-6 Pa•s, and the percent error was less than 0.6%. The maximum
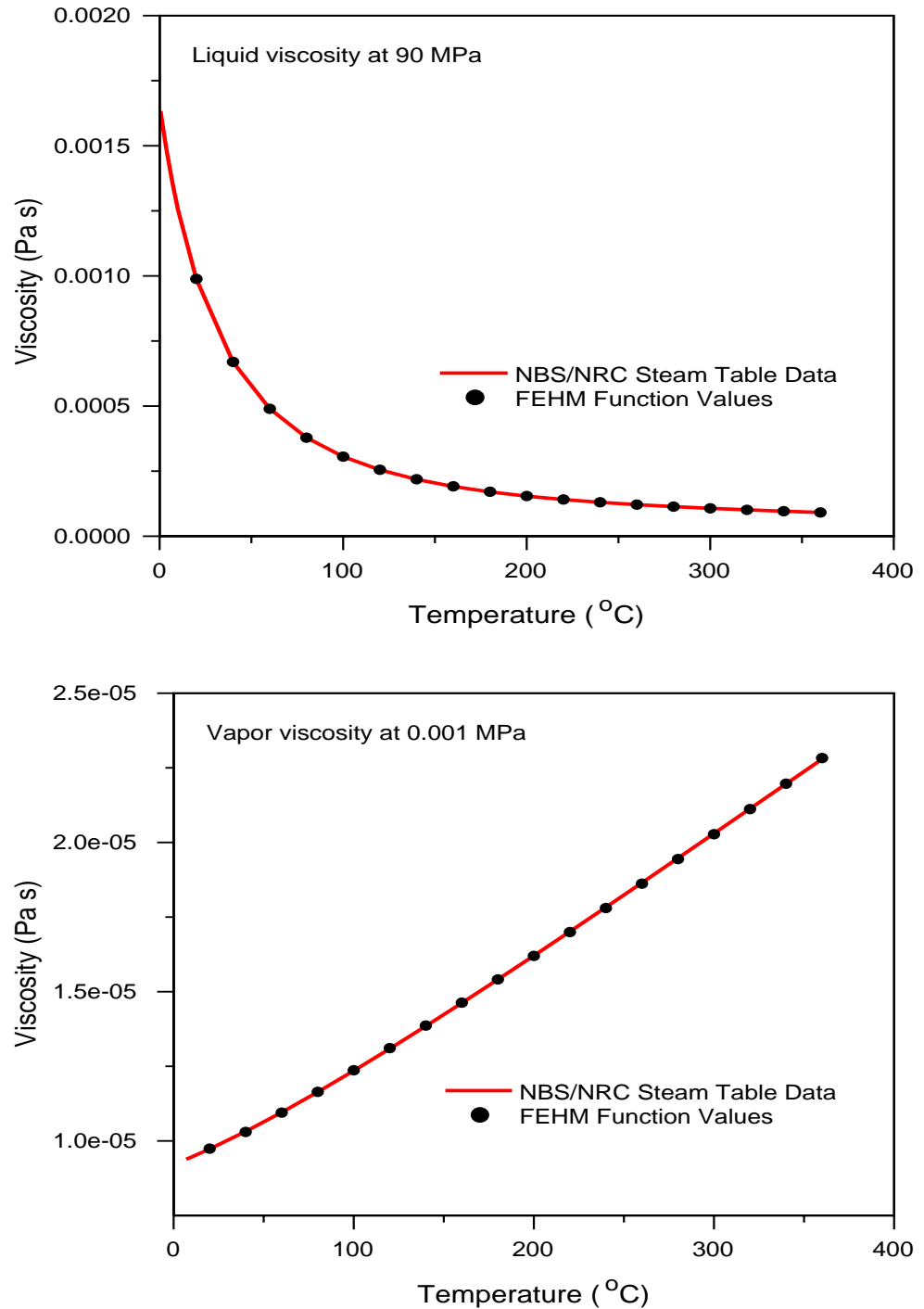
Figure 4. Comparison of FEHM viscosities to National Bureau of Standards Steam Table Data.

absolute error for vapor viscosity was 3.65e-8 Pa•s, and the percent error was less than 0.2%. These results meet the acceptance criteria for this test suite as developed in the FEHM VTP.

A spot check of liquid viscosities calculated for temperatures below 15 °C, indicates that errors will slightly exceed the acceptance criteria when pressures are below 6 MPa, and temperatures are below 3 °C. For a temperature of 0.5°C, at a pressure of 0.001 MPa the error in viscosity was 4.9e-5 Pa•s, 2.75 % of the steam table value. Errors for vapor viscosities calculated for temperatures below 15 °C, at a pressure of 0.001 MPa also exceeded the acceptance criteria. For a temperature of 7 °C, at a pressure of 0.001 MPa the error in vapor viscosity was 8.3e-7 Pa•s, 8.9 % of the steam table value.

2.1.5 Saturation Pressure and Temperature

These tests verify that the FEHM saturation functions provide accurate values of pressure and temperature as illustrated in Figure 5. The results, compared numerically to the values used to generate the saturation functions (found in file thermo.saturation_data), are given in Table I. The maximum absolute error for saturation pressure was less than 0.03 MPa, and the percent error was 0.3%. The maximum absolute error for saturation temperature was 1.1 °C, and the percent error was 0.4%. These results meet the acceptance criteria for this test suite as developed in the FEHM VTP.
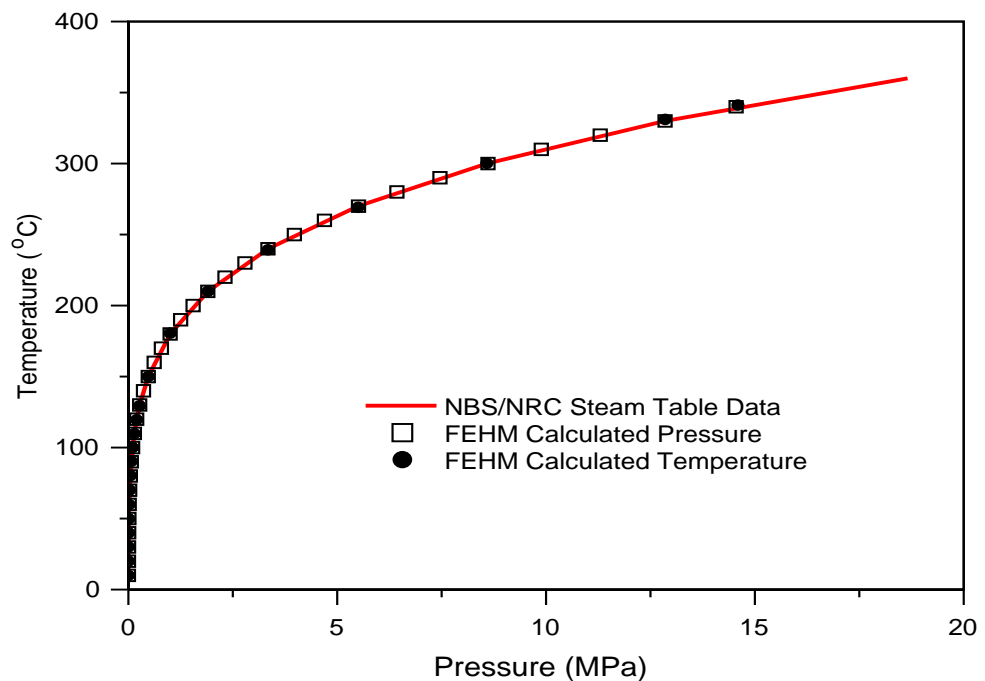
Figure 5. Comparison of FEHM saturation pressures and temperatures to National Bureau of Standards Steam Table Data.

2.2 Test of Heat Conduction

2.2.1 2-D Heat Conduction in a Square

These tests verify that FEHM correctly models 2-dimensional heat conduction. They also verify that the finite element representation of 2-D 3-node triangles (triangular element meshes), 4-node quadrilaterals (rectangular element meshes), mixed element meshes (containing both triangular and rectangular elements), and refined element meshes (containing rectangular and trapezoidal elements) have been correctly implemented. Figures 6 and 7 show that FEHM results are in good agreement with the analytical solution for the 2-D heat conduction simulations. The results, compared numerically to the analytical solution (found in files heat2dout.analyt_pos and heat2dout.analyt_time) are given in Table II. The maximum absolute error for these four runs was less than 0.9 °C, and the percent errors were less than 0.5%. These results meet the acceptance criteria for this test suite as developed in the FEHM VTP.

Table II. Results of the 2-D Heat Conduction Test			
V&V Test	Maximum Error	Maximum % Error	RMS Error
Temperature vs. time at x = y = 0.0 m			
3-node triangles	0.5805	0.4162	7.661e-05
4-node quadrilaterals	0.7140	0.3666	4.060e-05
mixed elements	0.5530	0.2815	5.129e-05
refined elements	0.8345	0.4313	4.253e-05
Temperature vs. position at t = 2.16e4 seconds			
3-node triangles	0.5978	0.3423	7.415e-04
4-node quadrilaterals	0.7066	0.3649	8.162e-04
mixed elements	0.6671	0.3466	7.644e-04
refined elements	0.8615	0.4452	8.725e-04

2.2.2 3-D Heat Conduction in a Cube

These tests verify that FEHM correctly models 3-dimensional heat conduction. They also verify that the finite element representation of 3-D 6-node triangular prisms (prism elements), 8-node quadrilateral polyhedrons (brick elements), 4-node tetrahedrals, mixed element meshes (containing both triangular prisms and quadrilateral polyhedrons), and refined element meshes (containing quadrilateral polyhedrons and trapezoidal polyhedrons) and the finite volume option have been correctly implemented. Figures 8 and 9 show that FEHM results are in good agreement with the analytical solution for the 3-D heat conduction simulations. The results, compared numerically to the analytical solution (found in files heat3dout.analyt_pos and heat3dout.analyt_time) are given in Table III. The maximum absolute error for these seven runs was less than 1.3 °C, and the percent errors were less than 0.7%. These results meet the acceptance criteria for this test suite as developed in the FEHM VTP.
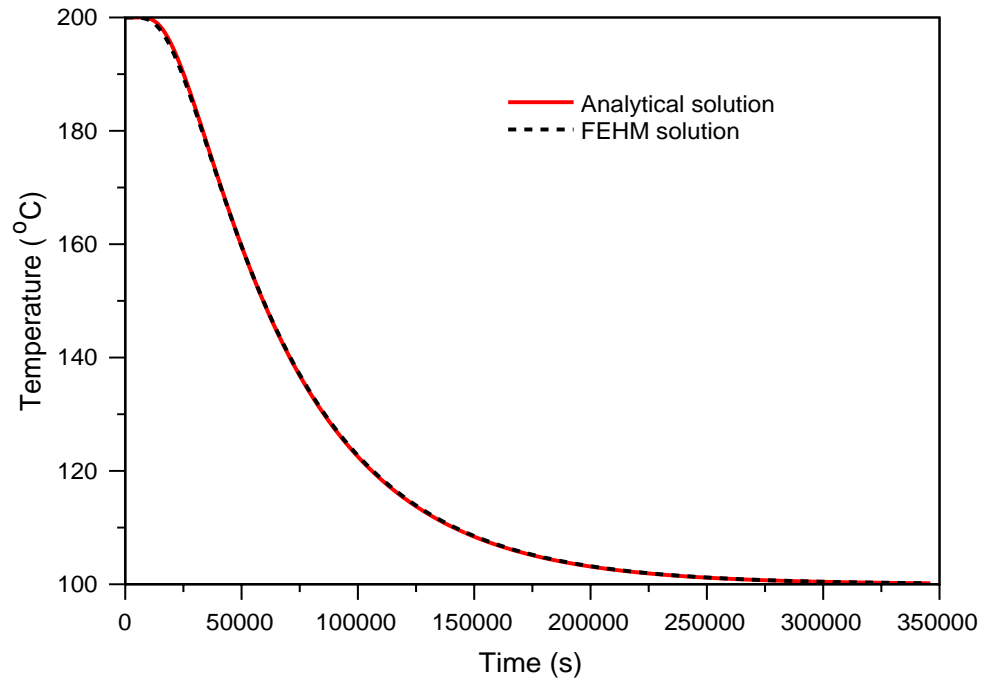
Figure 6.   Comparison of FEHM and analytical solutions for 2-D heat conduction at coordinate position x = y = 0 m.
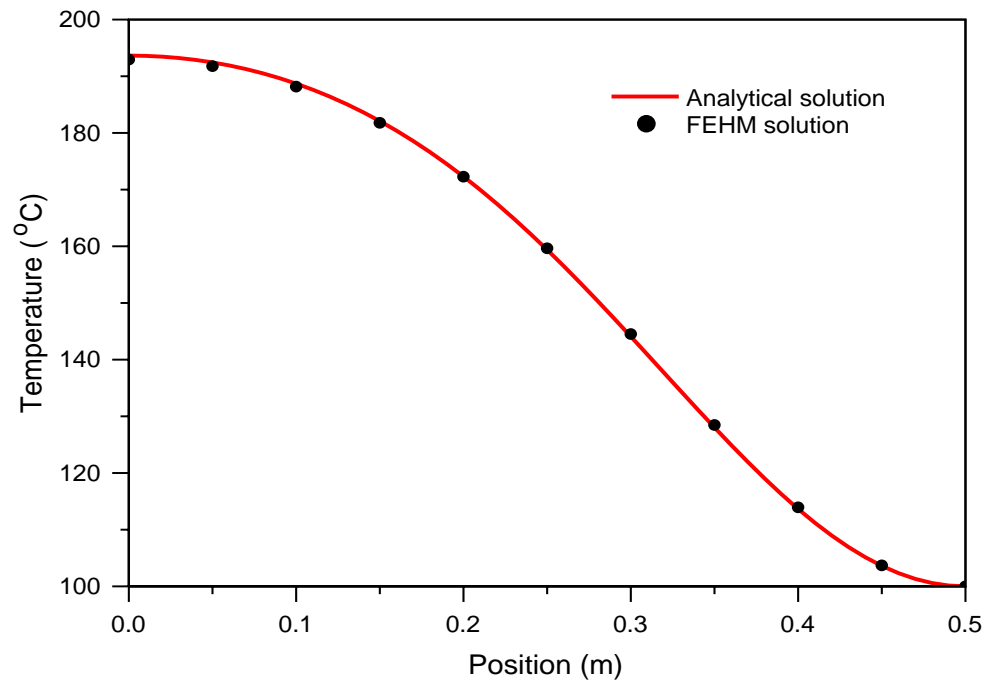
Figure 7.   Comparison of FEHM and analytical solutions for 2-D heat conduction at time t = 2.16e4 seconds.
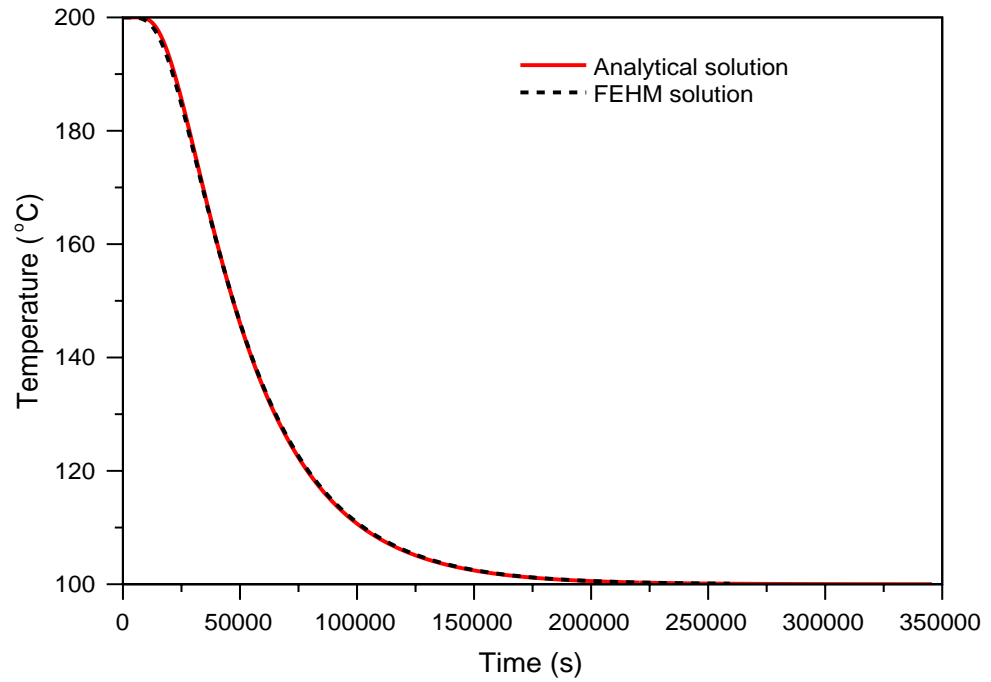
Figure 8.   Comparison of FEHM and analytical solutions for 3-D heat conduction at coordinate position x = y = z = 0 m.
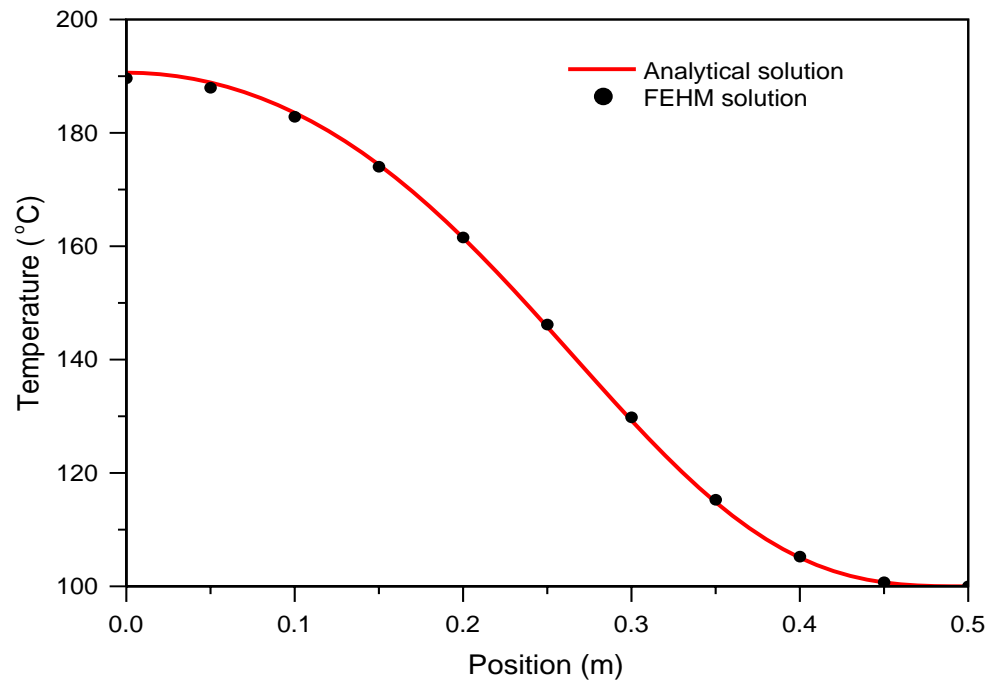
Figure 9.   Comparison of FEHM and analytical solutions for 3-D heat conduction at time t = 2.16e4 seconds.

Table III. Results of the 3-D Heat Conduction Test			
V&V Test	Maximum Error	Maximum % Error	RMS Error
Temperature vs. time at x = y = z = 0.0 m			
6-node triangular prisms	0.7860	0.5670	1.164e-04
8-node quadrilateral polyhedrons	1.0190	0.5275	6.811e-05
4-node tetrahedral	1.2450	0.6520	7.690e-05
mixed elements	0.8470	0.4349	7.936e-05
refined elements	1.2670	0.6632	7.874e-05
8-node quadrilateral polyhedrons with finite volume option	1.0190	0.5275	6.811e-05
refined elements with finite volume option	1.0320	0.5343	6.892e-05
Temperature vs. position at t = 2.16e4 seconds			
6-node triangular prisms	0.7957	0.5284	1.056e-03
8-node quadrilateral polyhedrons	0.9912	0.5200	1.065e-03
4-node tetrahedral	1.2430	0.6523	1.157e-03
mixed elements	0.8211	0.4403	9.982e-04
refined elements	1.2650	0.6634	1.124e-03
8-node quadrilateral polyhedrons with finite volume option	0.9912	0.5200	1.065e-03
refined elements with finite volume option	1.0050	0.5273	1.075e-03

2.3   Test of Temperature in a Wellbore

This test verifies that FEHM has correctly implemented the heat and mass transfer problem and 2-D radial geometry. Figures 10 and 11 show that FEHM results are in good agreement with the analytical solution. The results, compared numerically to the analytical solution (found in files rameyout.analyt_pos and rameyout.analyt_time) are given in Table IV. The maximum absolute error for this run was less than 1.4 °C, and the percent errors were less than 3%. These results meet the acceptance criteria for this test suite as developed in the FEHM VTP.

Table IV. Results of the Temperature in a Wellbore Test			
V&V Test	Maximum Error	Maximum % Error	RMS Error
Temperature vs. time			
d = 0 m	2.573e-02	0.1286	3.112e-05
d = 1000 m	1.3450	2.8150	1.556e-03
d = 2000 m	1.0570	1.3580	1.061e-03
Temperature vs. depth			
t = 25 days	0.6971	1.0260	5.203e-04
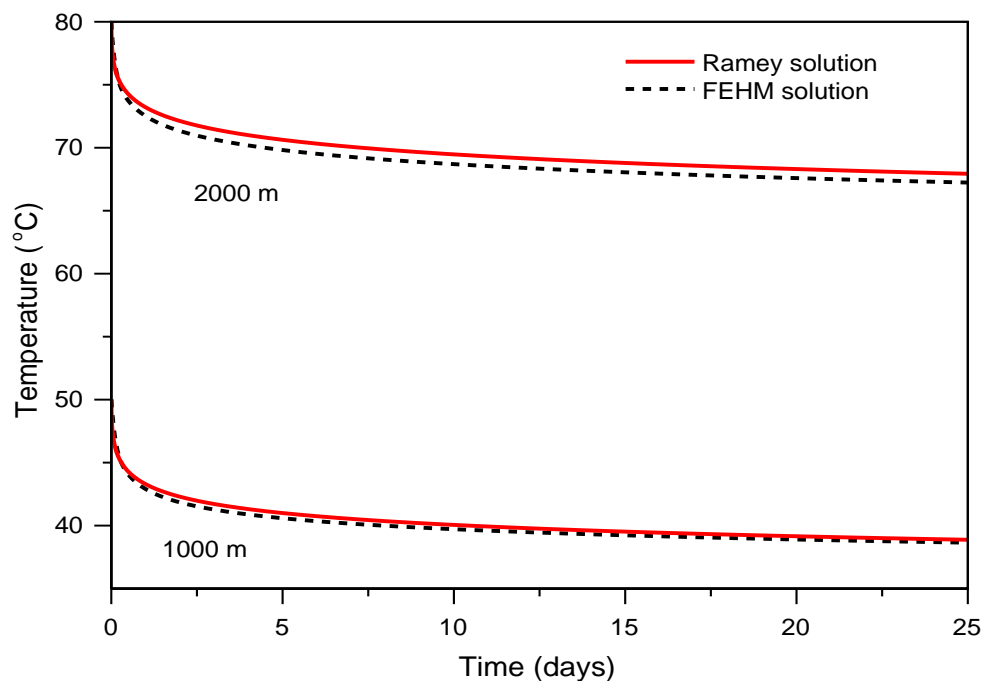
Figure 10. Comparison of FEHM and Ramey analytical solutions for temperature vs. time at d = 1000 m and d = 2000 m.
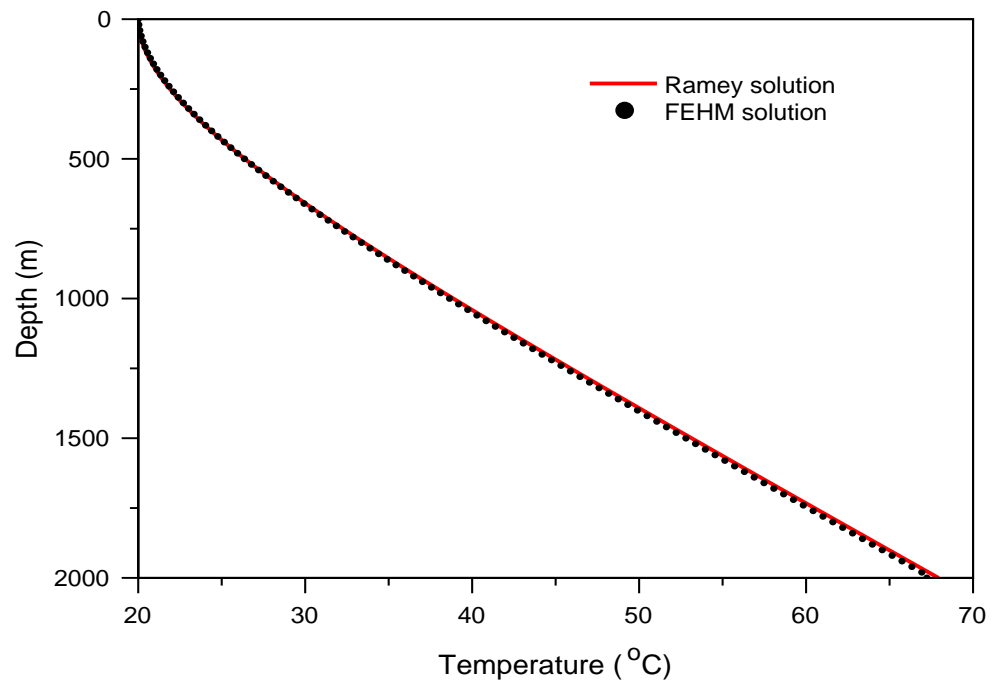
Figure 11. Comparison of FEHM and Ramey analytical solutions for temperature vs. depth at t = 25 days.

2.4   Test of Hydraulic Head

This test verifies that FEHM has correctly implemented the pressure equations, and that head and pressure formulations for a saturated problem yield the same solution for the same problem. Figure 12 shows that the FEHM results for the head and pressure formulations are in good agreement. The results, compared numerically, are given in Table V. The maximum absolute error for this simulation was less than 0.0005 MPa, the percent errors were less than 0.04%, and the RMS errors were less than 0.0002. These results meet the acceptance criteria for this test suite as developed in the FEHM VTP.

Table V. Results of the Hydraulic Head Test			
V&V Test	Maximum Error	Maximum % Error	RMS Error
Pressure vs. position at t = 365 days			
Depth 0 meters	4.116e-04	3.010e-02	1.505e-04
Depth 25 meters	2.606e-04	2.321e-02	1.160e-04
Depth 50 meters	1.419e-04	1.614e-02	8.072e-05
Depth 75 meters	5.531e-05	8.714e-03	4.357e-05
Depth 100 meters	9.260e-07	2.371e-04	1.185e-06
Node by node comparison	4.116e-04	3.010e-02	1.702e-05
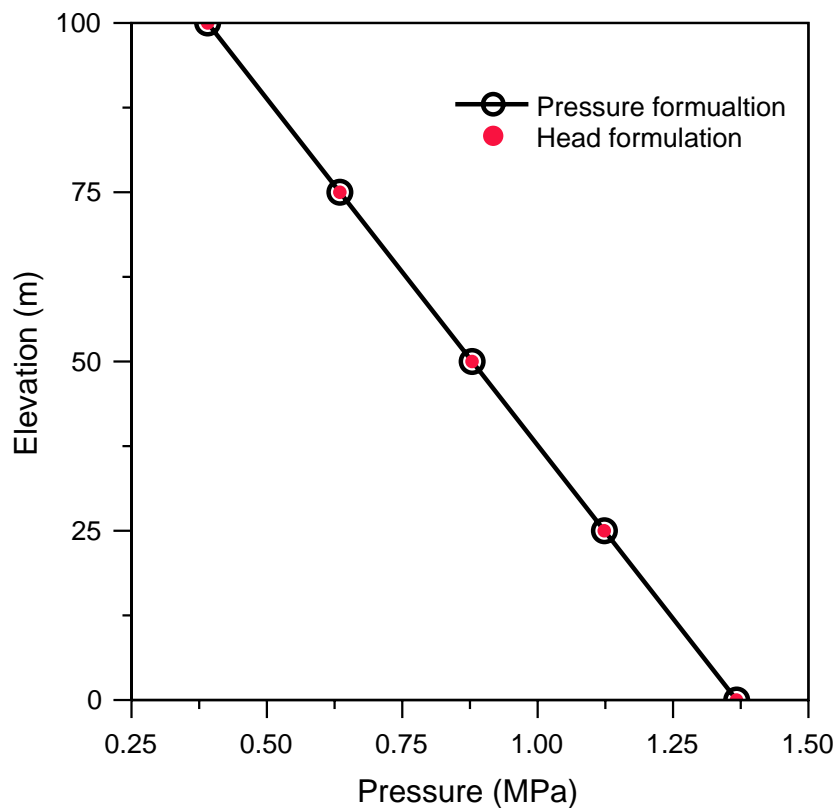
Figure 12. Comparison of FEHM head and pressure formulations for pressure vs. elevation at t = 365 days.

2.5   Test of Pressure Transient Analysis

This test verifies that FEHM has correctly implemented the pressure equations, i.e., the conservation of mass with Darcy's law, and that radial geometry has been correctly implemented. Figures 13 and 14 show that the FEHM results are in good agreement with the analytical solution. The results, compared numerically to the analytical solution (found in files theisout.analyt_pos and theisout.analyt_time) are given in Table VI. The maximum absolute error for this simulation was less than 0.00002 MPa, and the percent errors were less than 0.002%. These results meet the acceptance criteria for this test suite as developed in the FEHM VTP.

Table VI. Results of the Pressure Transient Analysis Test			
V&V Test	Maximum Error	Maximum % Error	RMS Error
Pressure vs. time			
at r = 0.00144 m	1.101e-05	1.100e-03	6.681e-08
at r = 3.44825 m	6.010e-06	6.010e-04	7.722e-08
Pressure vs. position			
at t = 1 day	2.843e-06	2.842e-04	1.742e-07
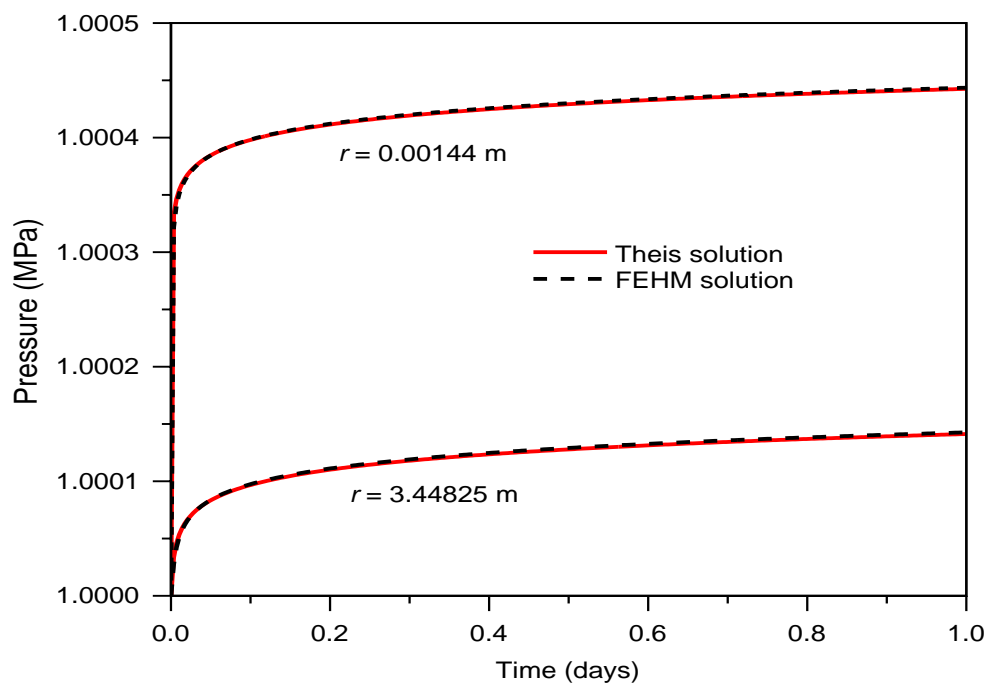
Figure 13. Comparison of FEHM and Theis solutions for pressure vs. time at r = 0.00144 m and r = 3.44825 m from the wellbore.
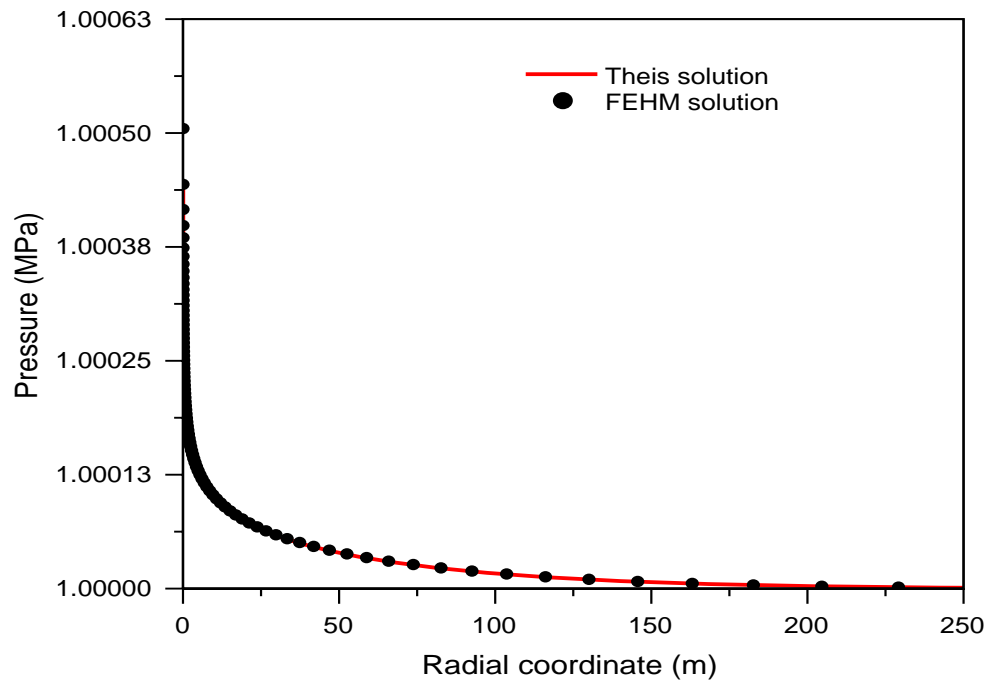
Figure 14. Comparison of FEHM and Theis solutions for pressure vs. position at *t* = 1 day.

2.6　Test of Simplified Water Table Calculations

This test verifies that FEHM has correctly implemented the simplified water table approximation. Figure 15 shows that the FEHM results for the UZ and WTSI formulations are in good agreement. The results, compared numerically, are given in Table VII. The RMS error for water table position was less than 0.01 and the total water budget was within 1%. These results meet the acceptance criteria for this test suite as developed in the FEHM VTP.

| Table VII.　Results of the Simplified Water Table Calculations Test			
V&V Test	Maximum Error	Maximum % Error	RMS Error
Water table position at $t = 365.25*10^6$ days			
Saturation 0.5	106.10	24.9000	8.164e-03
Total Water in System (kg)			
UZ Model	WTSI Model	Difference	% Error (of UZ Total)
1.801870e+09	1.786570e+09	1.530000e+07	0.8491
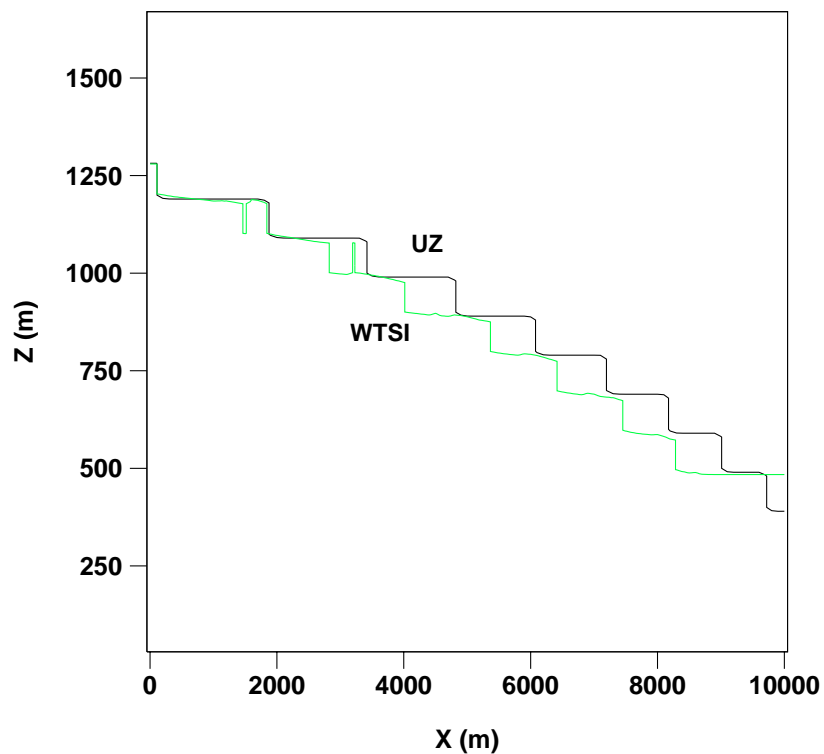
Figure 15.　Comparison of FEHM water table position for UZ and WTSI models for saturation = 0.5, at $t = 365.25*10^6$ days.

2.7 Test of Infiltration into a One-Dimensional, Layered, Unsaturated Fractured Medium

This test verifies that FEHM has correctly simulated the saturation profile for the infiltration into a one-dimensional, layered, unsaturated fratured medium. Figures 16, 17, and 18 show that the FEHM results are in good agreement with the TOUGH2 simulations. Please note that the expanded saturation scale in Fig. 18 exaggerates differences in fracture saturation at low elevations. The results for the equivalent continuum method (ECM) and double porosity/double permeability method (DPM), compared numerically to results from TOUGH2 (found in files infiltration.tough2.ecm, infiltration.tough2.fracture, and infiltration.tough2.matrix), are shown in Table VIII. The RMS error for the equivalent continuum model simulation was less than 1%, and the maximum percent error was less than 7%. As expected, significant deviations existed at material interfaces for the double porosity/double permeability model. These were the result of differences in model formulation for the fracture-matrix interaction terms. It should also be noted that the van Genuchten capillary pressure functions are singular at $S = 0$ and all codes must use extrapolation techniques to model values approaching 0. Differences in the extrapolation had the greatest effect on the fracture saturations which approach liquid residual values in the lowest zone. Although the maximum percent errors for the double porosity/double permeability model were large, the RMS errors for this simulation were less than 4%. These results meet the acceptance criteria for this test suite as developed in the FEHM VTP.

| Table VIII. Results of the Infiltration into a One-Dimensional, Layered, Unsaturated Fractured Medium Test			
V&V Test	Maximum Error	Maximum % Error	RMS Error
Saturation vs. elevation			
ECM	5.639e-02	6.1690	1.423e-03
DPM - Matrix saturation	8.151e-02	17.1200	2.068e-03
DPM - Fracture saturation	1.022e-02	355.0000	3.679e-02
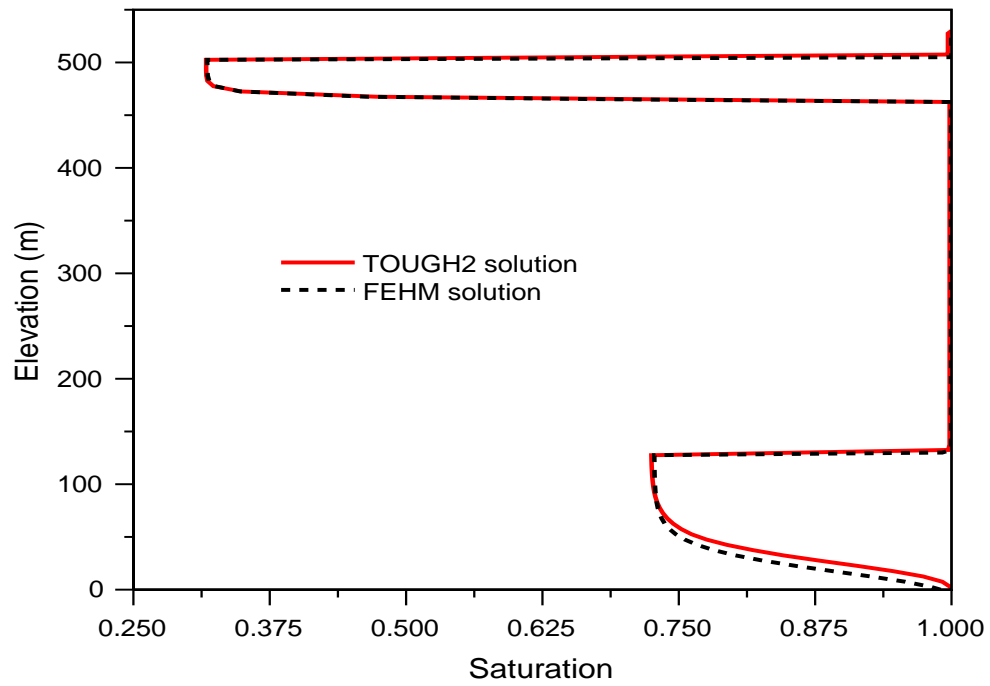
Figure 16. Comparison of FEHM and TOUGH2 saturations for an equivalent continuum model.
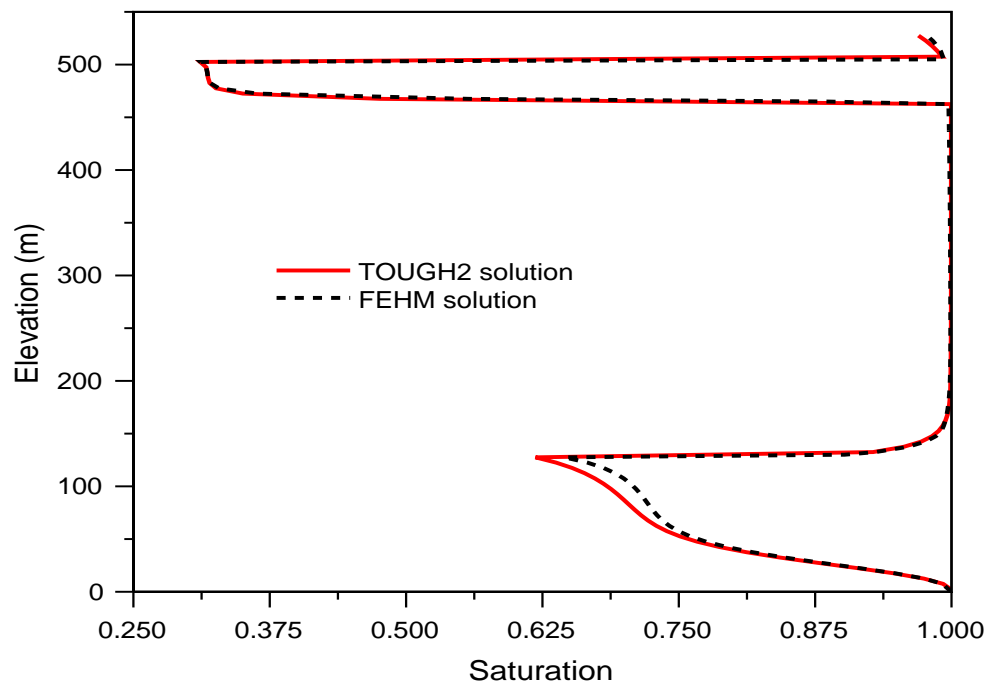
Figure 17. Comparison of FEHM and TOUGH2 matrix saturation for a double porosity/double permeability model.
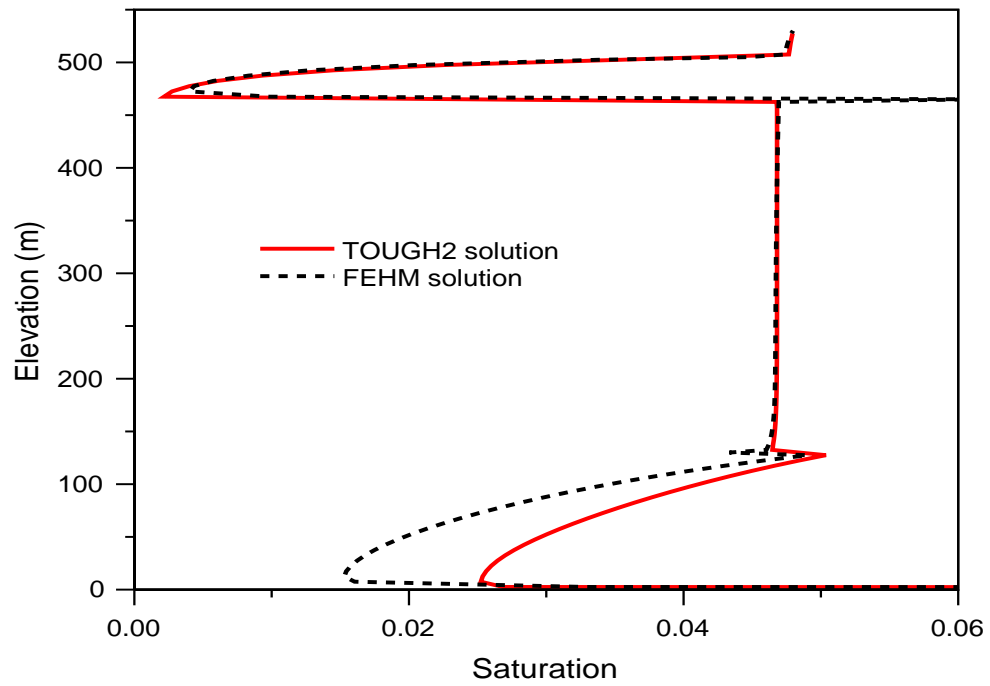
Figure 18. Comparison of FEHM and TOUGH2 fracture saturation for a double porosity/double permeability model.

2.8 Test of Vapor Extraction from an Unsaturated Reservoir

This test verifies that FEHM has correctly implemented steady state gas flow in a 2-D radial system with an isotropic and an anisotropic permeability model. Figures 19 and 20 show that FEHM results are in good agreement with the analytical solutions (found in files vapextractout_aniso.analyt and vapextractout_iso.analyt) for the vapor extraction simulations. The results of the numerical comparison to the analytical solutions are given in Table IX. The maximum absolute error in vapor pressure for the isotropic case was less than 0.002 MPa and for the anisotropic case was less than 0.004 MPa, the maximum percent errors were less than 4% and the RMS errors were less than 0.01 for both models. These results meet the acceptance criteria for this test suite as developed in the FEHM VTP.
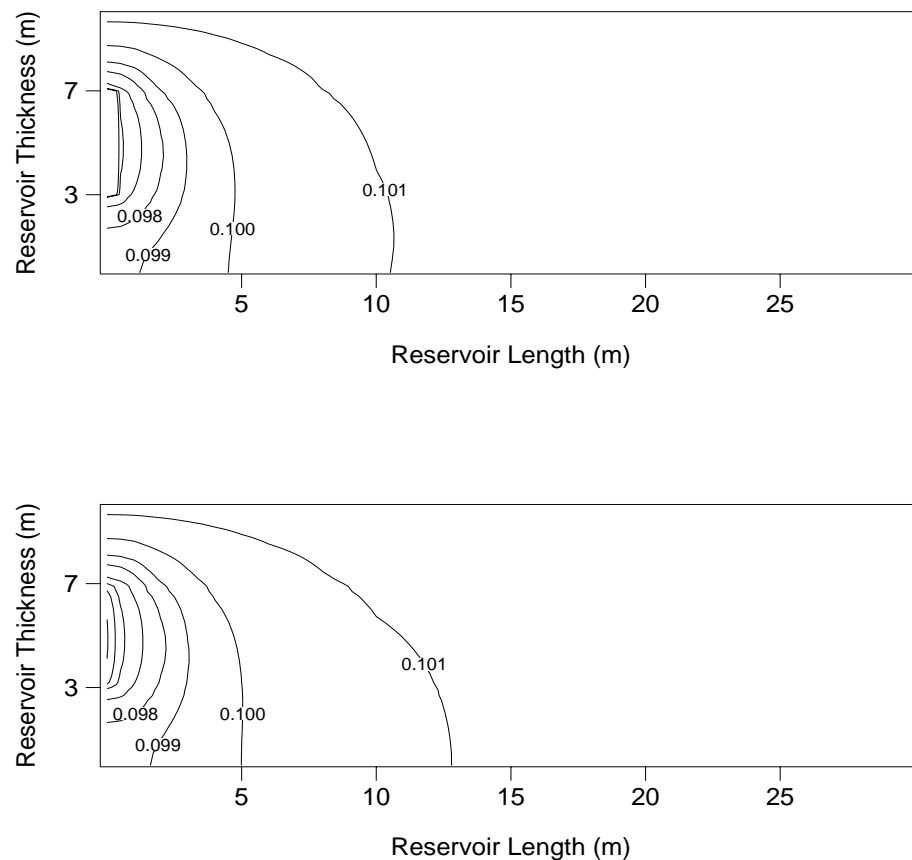
Figure 19. Comparison of FEHM steady state vapor pressure (top) with Shan analytical solution (bottom) for an isotropic reservoir.
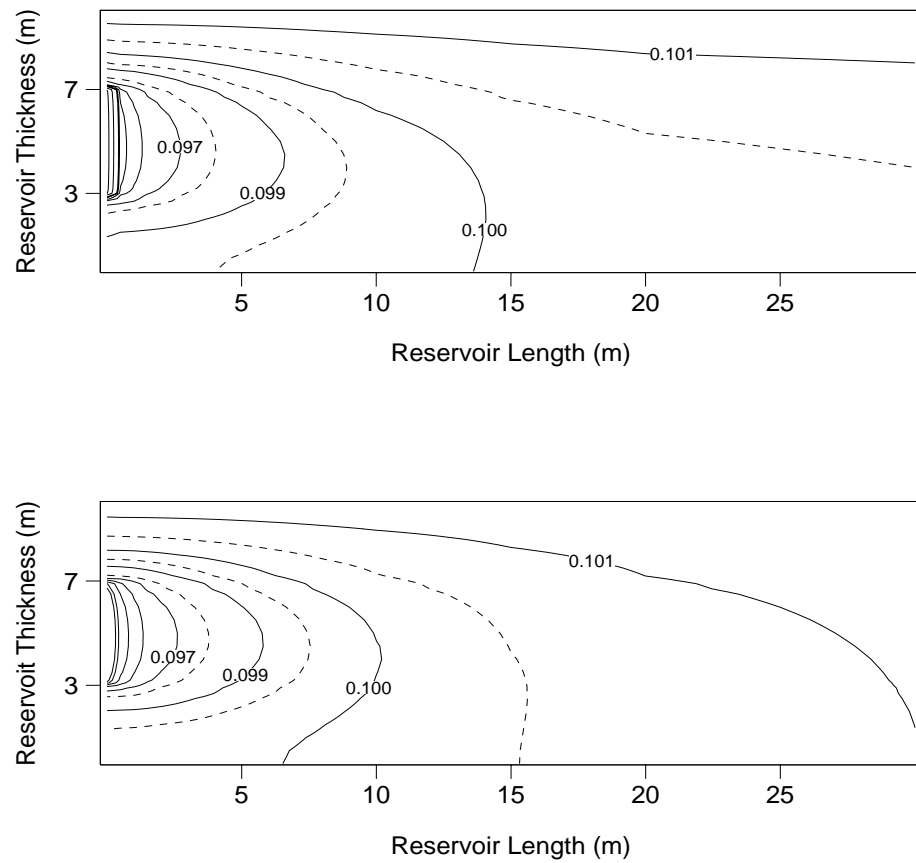
Figure 20. Comparison of FEHM steady state vapor pressure (top) with Shan analytical solution (bottom) for an anisotropic reservoir.

Table IX. Results of the Vapor Extraction from an Unsaturated Reservoir Test			
V&V Test	Maximum Error	Maximum % Error	RMS Error
Vapor pressures at each node			
Isotropic case	1.983e-03	2.1950	8.838e-05
Anisotropic case	3.066e-03	3.3110	1.436e-04

2.9 Test of Barometric Pumping

This test verifies that FEHM correctly solves both the heat and mass transfer equation and the solute transport equation in one-dimension, for air flow and vapor-phase contaminants under an implied surface boundary condition that represents barometric pumping. Figure 21 shows that FEHM agrees well with Auer et al.'s semi-analytic solution for pore-velocity. The difference in pore-velocity seen near the surface is due to the linearization of the semi-analytic solution. Figure 22 shows that FEHM also agrees well with Auer et al.'s semi-analytic solution for solute transport. The results, compared numerically to the semi-analytical solutions (found in files auer_vel.analyt and auer_MFR.analyt) are given in Table X. Errors associated with the contaminant flux verification (i.e. mass fraction remaining) are related to the fact that Auer et al.'s (1996) numerical code is using about 280 zones vertically. FEHM is using 120 vertical zones. The grid size for FEHM was chosen because it provided good results with minimal program run time. The RMS error for the pore-scale velocity test was less than 0.008, and for the contaminant transport tests was less than 0.0005. These results meet the acceptance criteria for this test suite as developed in the FEHM VTP.

Table X. Results of the Barometric Pumping Tests			
V&V Test	Maximum Error	Maximum % Error	RMS Error
Pore-scale velocity test: Velocity vs. depth during pumping cycle			
1.75 days	3.354e-08	31.6100	7.241e-03
3.5 days	2.069e-07	49.0200	3.716e-03
5.25 days	1.878e-08	39.3000	4.515e-03
7 days	2.170e-07	48.0400	3.594e-03
Contaminant transport tests: Mass fraction remaining vs. time			
$\alpha = 0.0$	2.205e-03	0.2321	3.509e-04
$\alpha = 0.1$	5.226e-04	5.872e-02	8.311e-05
$\alpha = 0.2$	1.730e-03	0.1906	4.513e-04
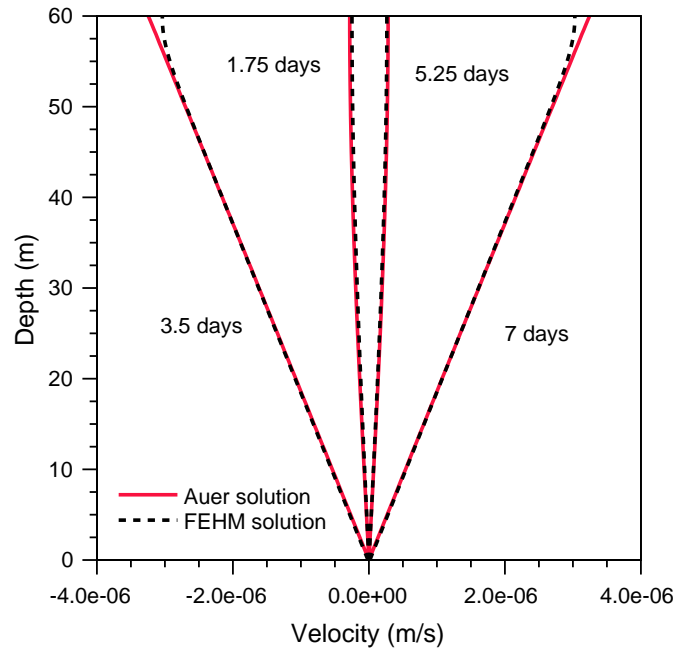
Figure 21. Comparison of FEHM pore-scale velocity with Auer semi-analytic solution.
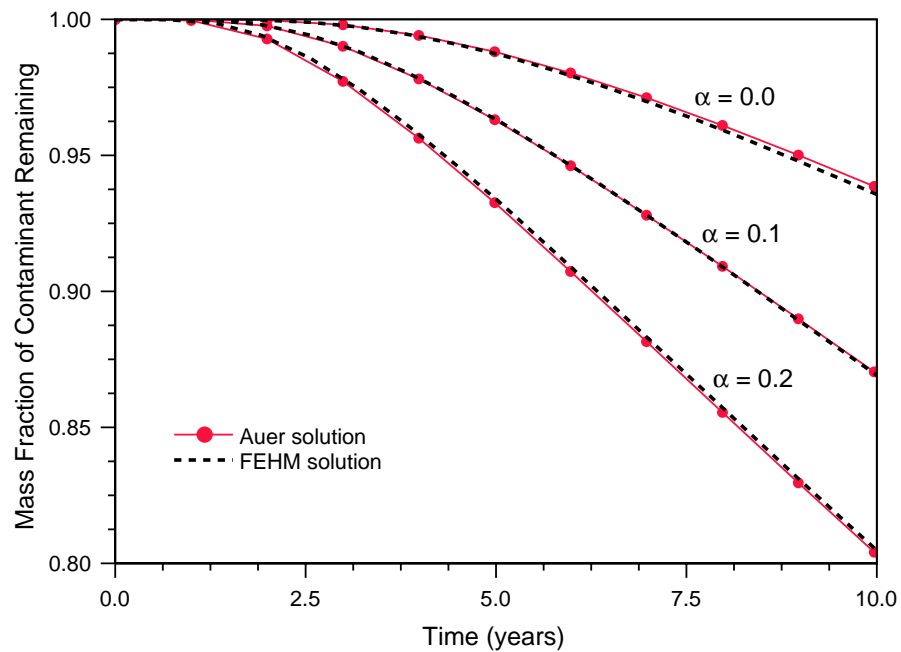
Figure 22. Comparison of FEHM solution for contaminant mass fraction remaining (MFR) with Auer analytical solution.

2.10 Test of Dual Porosity

This test verifies that FEHM has correctly implemented the dual porosity formulation. Figures 23, 24, and 25 show that FEHM results are in good agreement with the analytical solution for the dual porosity simulations. The differences between the analytical and FEHM solutions can be attributed primarily to the fact that the analytical solution uses a steady state approximation for the matrix flow (lumped 1 node) while FEHM uses a transient approximation (2 node) for the matrix material. The results, compared numerically to the analytical solution (found in files dual1_out.analyt, dual2_out.analyt, and dual3_out.analyt) are given in Table XI. The maximum absolute error for these three runs for nondimensional pressure was less than 0.038, and the percent errors were less than 1.2%. These results meet the acceptance criteria for this test suite as developed in the FEHM VTP.

Table XI. Results of the Dual Porosity Test			
V&V Test	Maximum Error	Maximum % Error	RMS Error
Dimensionless pressure drop vs. dimensionless time at $r_w = 0.17528$ m			
Case 1	3.784e-02	1.1770	7.994e-04
Case 2	1.858e-02	0.6075	5.318e-04
Case 3	1.995e-02	0.6331	5.482e-04
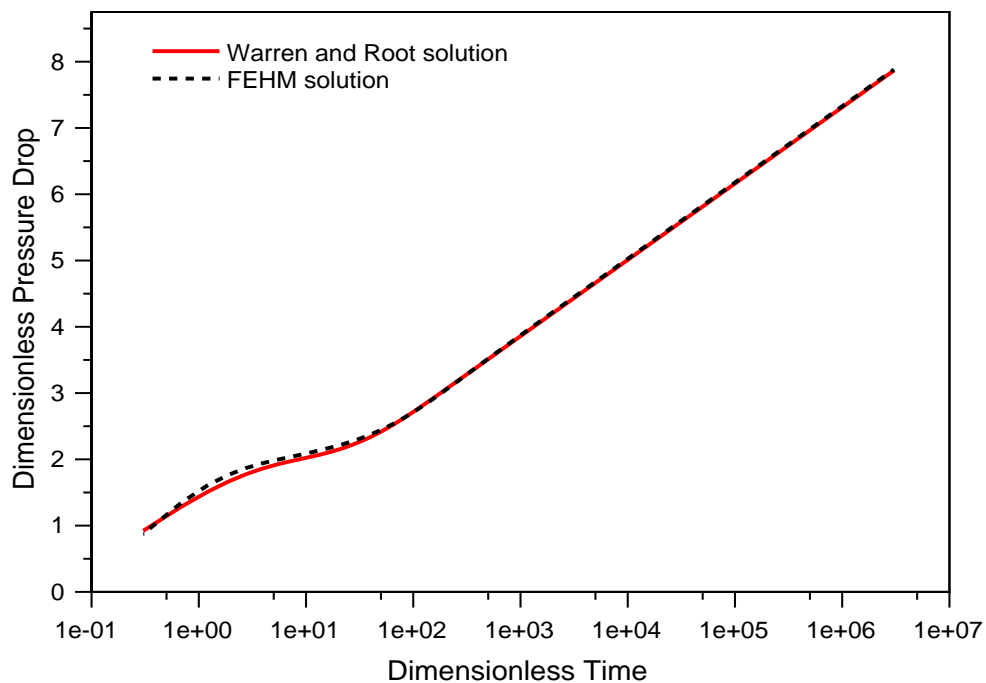
Figure 23. Comparison of FEHM and analytical solution for dual porosity case 1, $\lambda = 0.02546$, $\omega = 0.1000$.
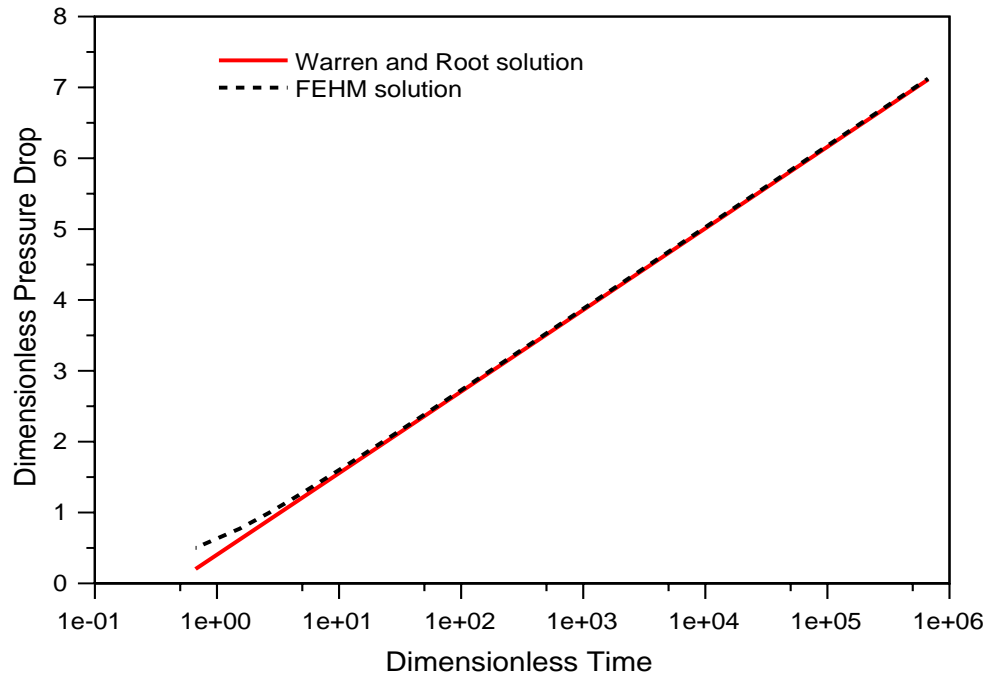
Figure 24. Comparison of FEHM and analytical solution for dual porosity case 2, $\lambda = 25.46,$ $\omega = 0.01099$ **.**
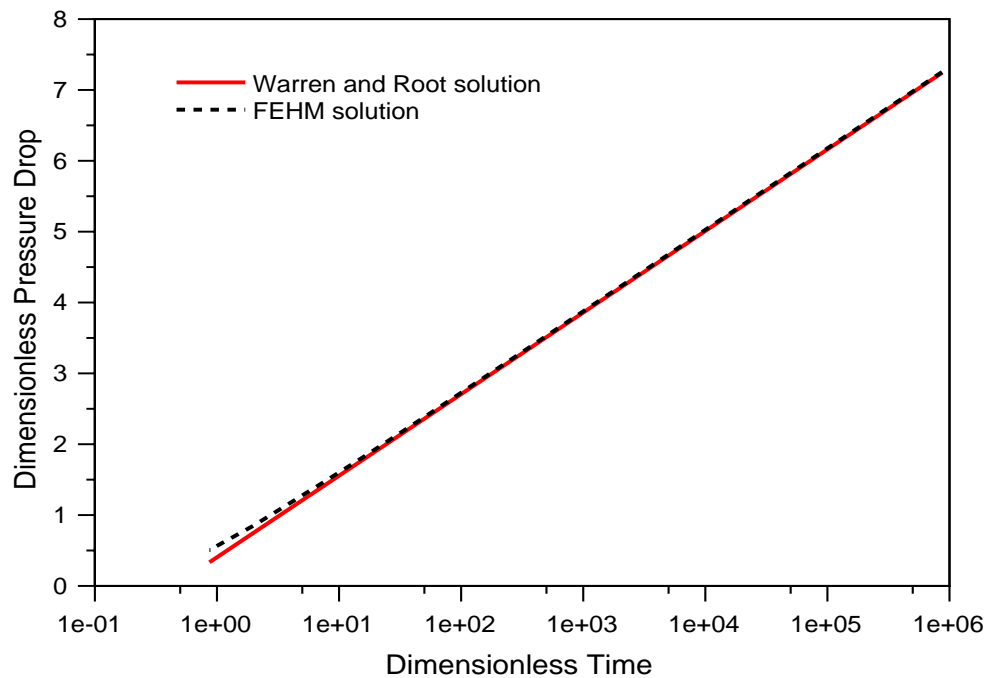
Figure 25. Comparison of FEHM and analytical solution for dual porosity case 3, $\lambda = 164.7,$ $\omega = 0.001013$ **.**

2.11 Test of Heat and Mass Transfer in Porous Media

This test suite verifies that the heat and mass transfer problem has been correctly formulated, that radial geometry has been correctly implemented and that finer meshes can improve accuracy. Figures 26 and 27 show that FEHM results are in good agreement with the analytical solution. For the 84-node test grid, mesh discretization errors are apparent. Other differences are probably due to slight differences in the calculation of thermodynamic properties (the analytical solution uses constant properties). The results, compared numerically to the analytical solution (found in files avdoninout.analyt_pos and avdoninout.analyt_time) are given in Table XII. The maximum absolute error for these three runs was less than 1.3 °C, and the percent errors were less than 0.8%. These results meet the acceptance criteria for this test suite as developed in the FEHM VTP.

Table XII. Results of the Heat and Mass Transfer in Porous Media Test			
V&V Test	Maximum Error	Maximum % Error	RMS Error
Temperature vs. time at r = 37.5 m			
84 Node Grid	1.2630	0.7775	2.169e-04
400 Node Grid	0.4062	0.2488	6.973e-05
800 Node Grid	0.3900	0.2383	6.742e-05
Temperature vs. position at t = 1.e9 seconds			
84 Node Grid	0.5233	0.3239	1.746e-04
400 Node Grid	0.2818	0.1745	3.417e-05
800 Node grid	0.2819	0.1746	2.214e-05
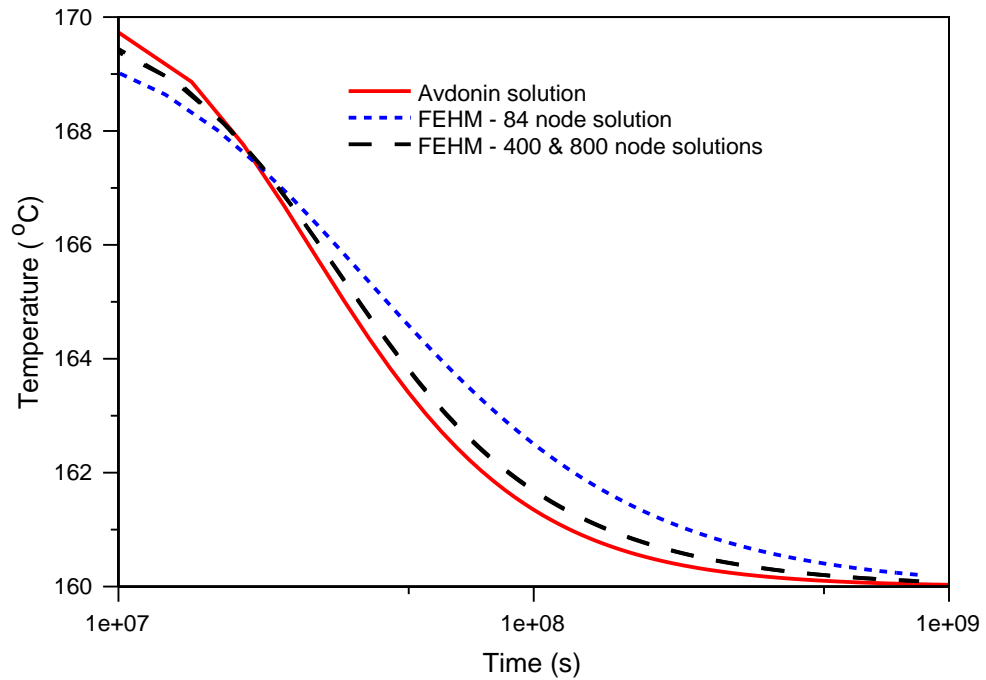
Figure 26. Comparison of FEHM and Avdonin analytical solutions for temperature vs. time at r = 37.5 m from injection well.
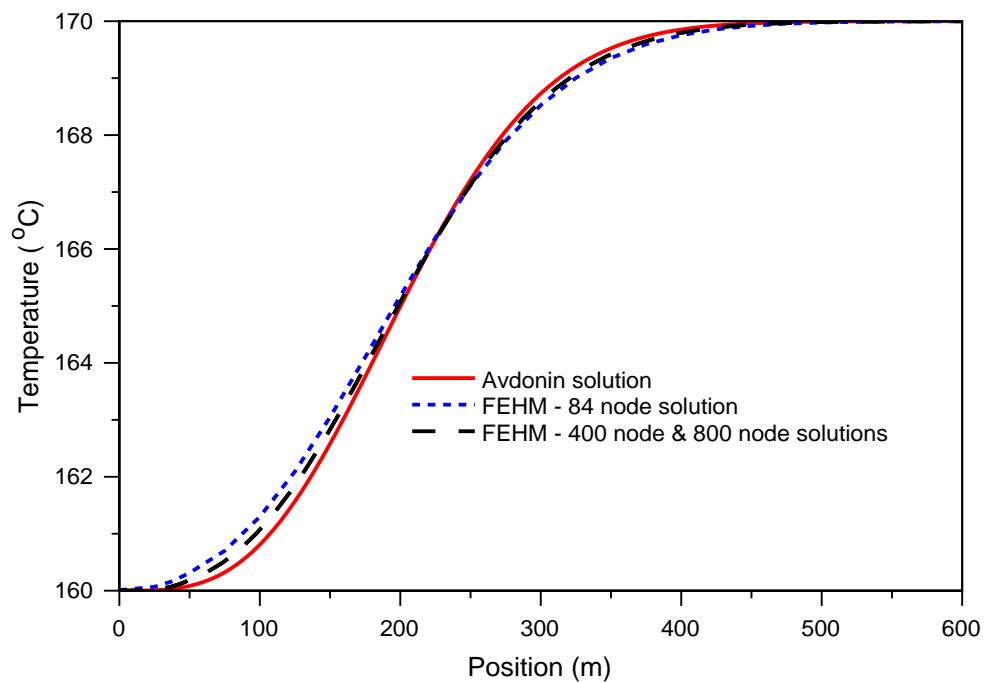
Figure 27. Comparison of FEHM and Avdonin analytical solutions for temperature vs. position at t = 1.e9 seconds.

2.12 Test of Free Convection

These tests verify that FEHM correctly models 2-dimensional free convection. Figures 28 and 29 show that FEHM generates convective cells for the 2-D free convection simulations. The results, compared numerically to the initial simulations (found in files conv2d_air_check.10002_sca_node conv2d_air_check.10002_vec_node, conv2d_water_check.10002_sca_node, and conv2d_water_check.10002_vec_node) are given in Table XIII. The maximum absolute error for temperature for these two runs was less than 0.06 °C, and the percent errors were less than 0.1%. The RMS errors for volume flux magnitude were less than 0.0005. These results meet the acceptance criteria for this test suite as developed in the FEHM VTP.

Table XIII. Results of the 2-D Free ConvectionTest			
V&V Test	Maximum Error	Maximum % Error	RMS Error
Temperature vs. position at t = 1.e6 days			
Air convection	5.947e-02	9.901e-02	9.589e-06
Water convection	2.255e-02	3.677e-02	2.820e-06
Volume flux magnitude vs. position at t = 1.e6 days			
Air convection	2.433e-06	3.428	4.262e-04
Water convection	2.387e-10	3.914	8.145e-05
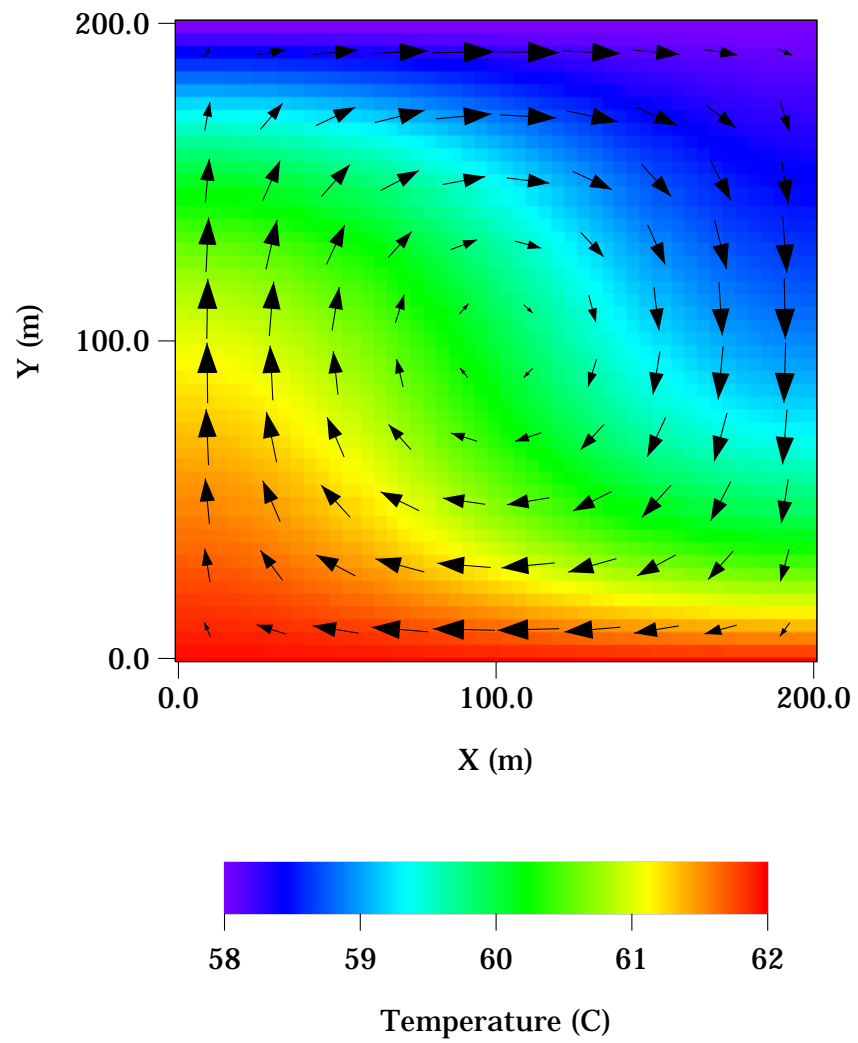
Figure 28. Illustration of FEHM temperature and vector field for free convection in air.
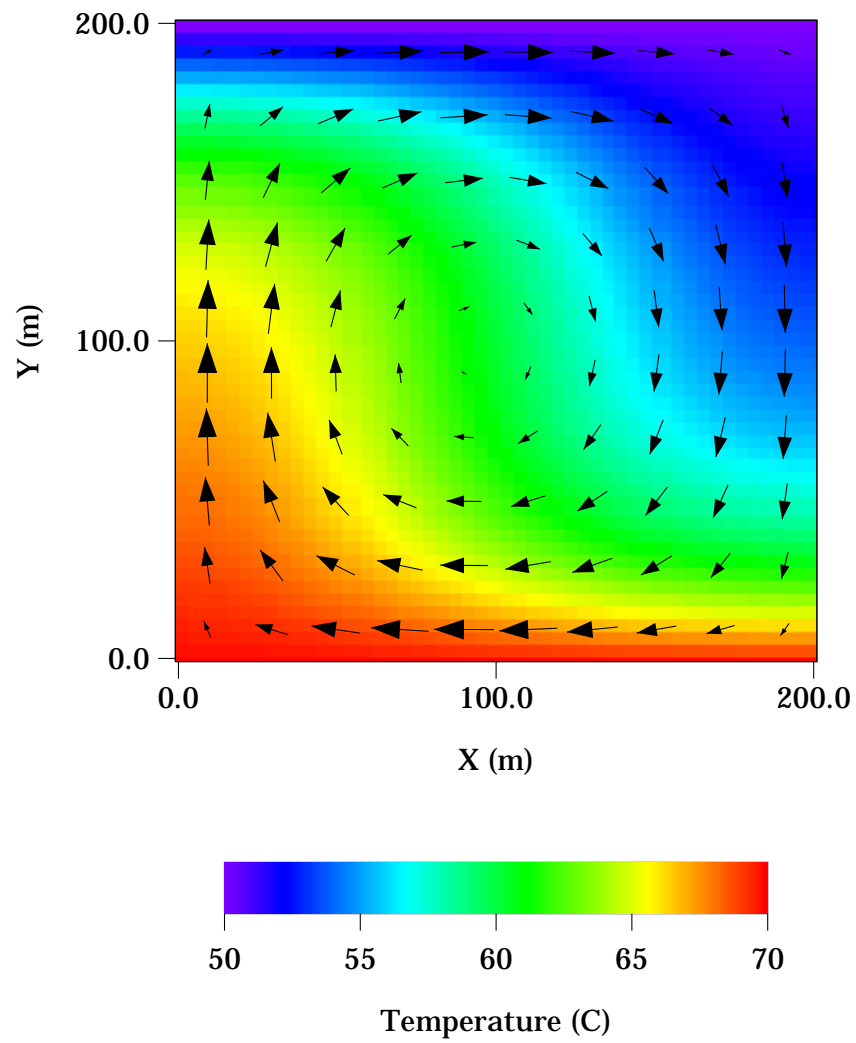
Figure 29. Ilustration of FEHM temperature and vector field for free convection in water.

2.13 Test of Toronyi Two-phase Problem

This test verifies that FEHM has correctly implemented heat and mass transfer and phase partitioning. Figure 30 shows the Toronyi and FEHM saturation fields for comparison. The results of the numerical comparison to the Thomas and Pierson (1978) solution (found in file toronyi.saturations) are given in Table XIV. The maximum absolute error in saturation for these runs was less than 0.002, and the percent errors were less than 2%. These results meet the acceptance criteria for this test suite as developed in the FEHM VTP.

Table XIV. Results of the Toronyi Two-phase Problem Test			
V&V Test	Maximum Error	Maximum % Error	RMS Error
Saturation at each central node at t= 78.31 days			
Coordinate grid	1.542e-03	1.3180	7.719e-04
FDM grid	1.641e-03	1.4020	8.652e-04
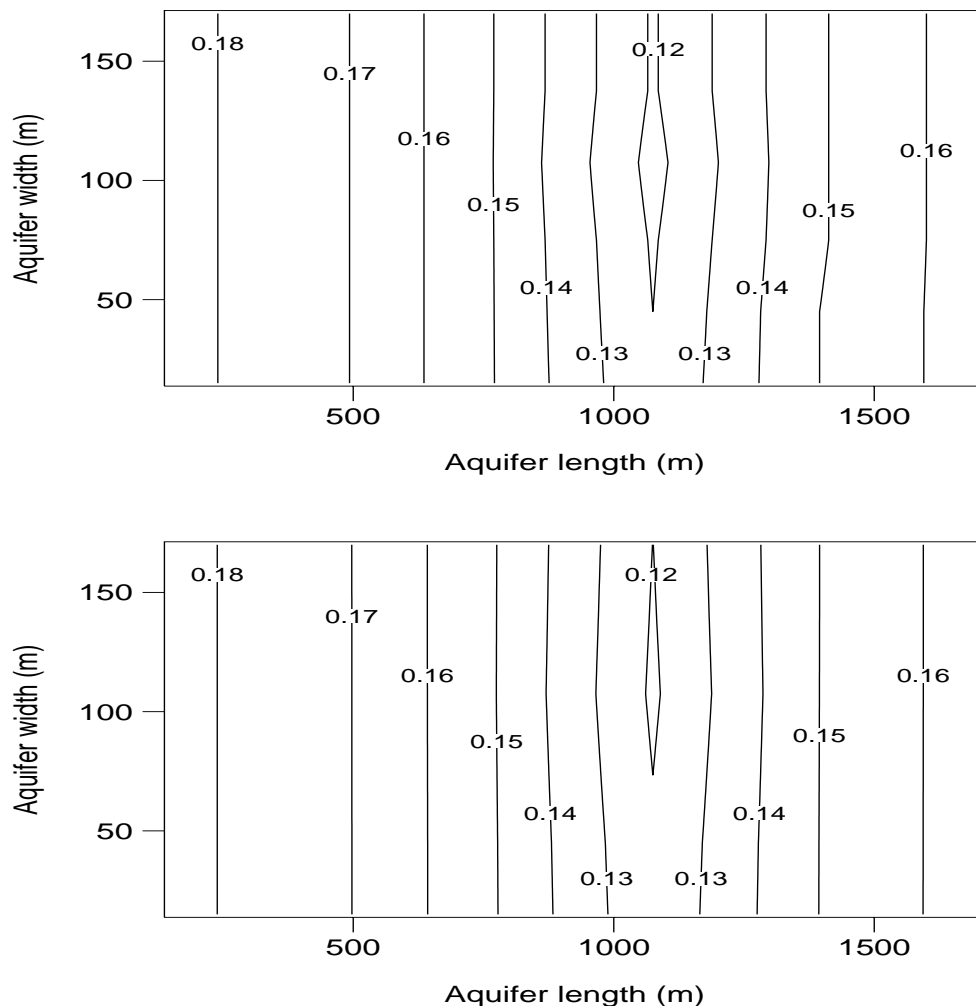
Figure 30. Comparison of Toronyi (top) and FEHM (bottom) saturation fields at t = 78.31 days.

2.14 Test of DOE Code Comparison Project Problem Five, Case A

This test verifies that FEHM has correctly implemented heat and mass transfer and phase partitioning. Figures 31 and 32 show that FEHM results are in good agreement with the other code solutions for the DOE Code Comparison Project Problem simulation. The results of the numerical comparison to the other code solutions are given in Table XV. The maximum absolute error in temperature at the production well for this run was less than 2.1 °C, the maximum absolute error in pressure at the production well for this run was less than 0.07 MPa, the maximum absolute error in pressure at the observation well for this run was less than 0.04 MPa, and the percent errors were all less than 3%. These results meet the acceptance criteria for this test suite as developed in the FEHM VTP.

Table XV. Results of the DOE Code Comparison Project Problem Test[‡]			
V&V Test	Maximum Error	Maximum % Error	RMS Error
Temperature at production node			
Code 1	1.3560	0.6532	7.746e-04
Code 2	1.5190	0.6471	1.070e-03
Code 3	1.6230	0.6867	1.259e-03
Code 4	2.0030	0.8528	1.139e-03
Code 5	1.4980	0.7299	9.932e-04
Code 6	1.3680	0.5906	1.379e-03
Pressure at production node			
Code 1	5.124e-02	1.5810	1.908e-03
Code 2	6.127e-02	2.0220	3.137e-03
Code 3	5.347e-02	1.7700	3.234e-03
Code 4	6.233e-02	2.0570	3.017e-03
Code 5	2.149e-02	0.7164	1.199e-03
Code 6	2.828e-02	0.9395	1.637e-03
Pressure at observation node			
Code 1	2.530e-02	0.7312	8.878e-04
Code 2	2.534e-02	0.7610	7.676e-04
Code 3	1.656e-02	0.4842	8.250e-04
Code 4	2.215e-02	0.6651	7.065e-04
Code 5	3.449e-02	1.0420	1.879e-03
Code 6	3.445e-02	1.0410	2.547e-03
[‡]Modelers Code 1 - Geotrans, Inc. Code 2 - Intercomp Code 3 - Lawrence Berkeley Laboratory (LBL) Code 4 - Systems, Science and Software (S-Cubed) Code 5 - Stanford University Code 6 - University of Auckland, New Zealand			
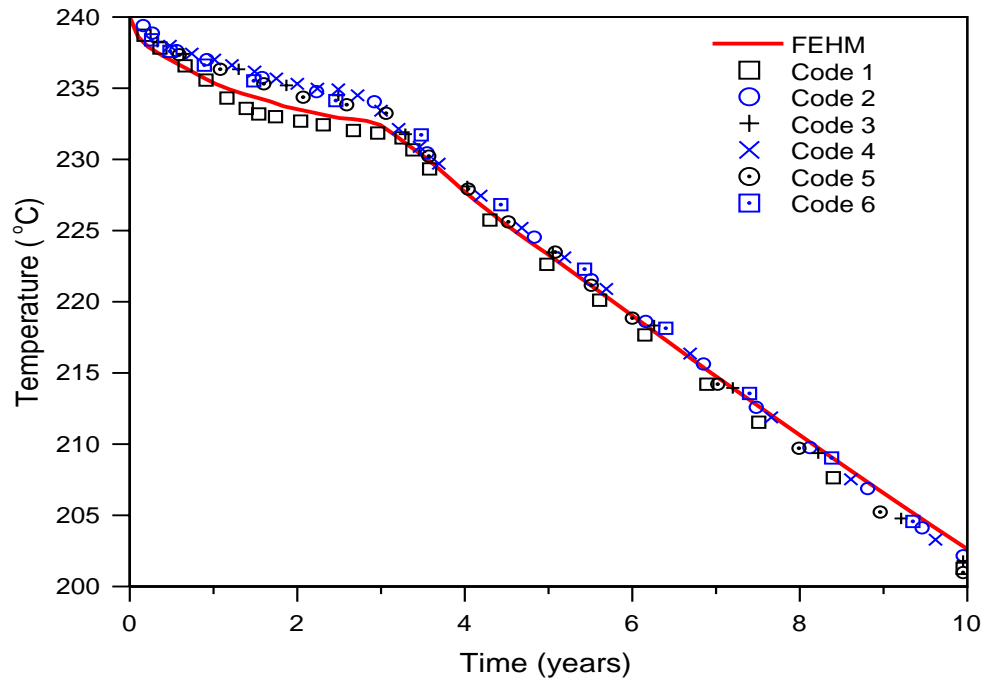
Figure 31. Comparison of FEHM production well temperatures with results from other codes.
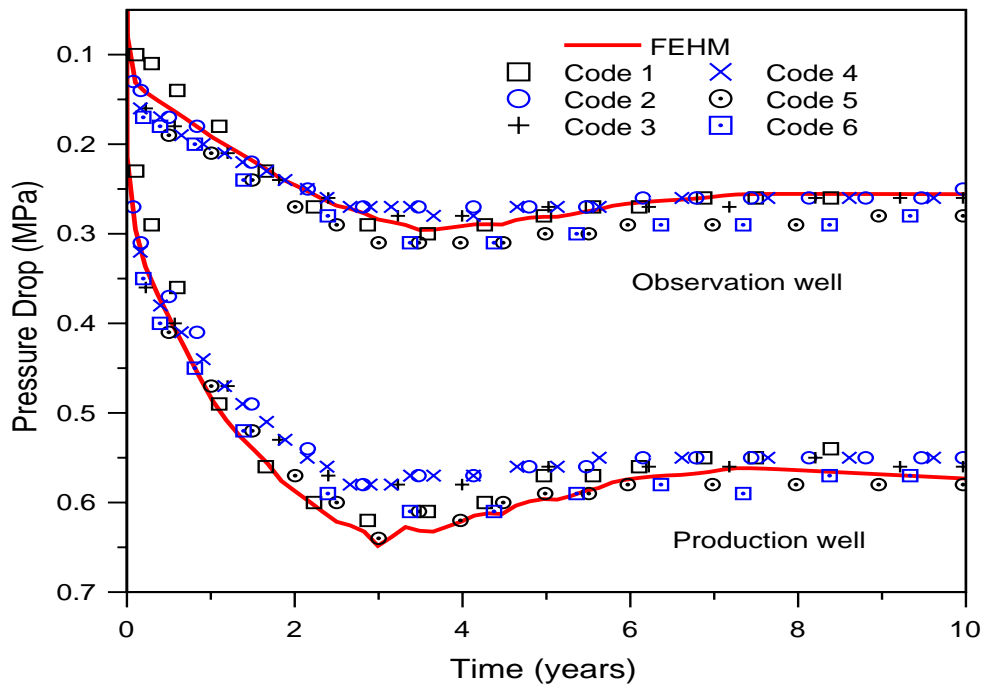
Figure 32. Comparison of FEHM production and observation well pressure drops with results from other codes.

2.15 Test of Heat Pipe

This test verifies that FEHM has correctly implemented the air-water-heat subsurface flow; unsaturated flow with high capillary forces; air-water vapor diffusion process; and finite difference(FDM) and finite element (FE) grids. The results, compared numerically, are given in Table XVI. The maximum absolute error for this simulation was less than $2*10^{-6}$ kg/s for vapor flux and $3*10^{-8}$ kg/s for liquid flux, the percent errors were less than 5 %, and the RMS errors were less than 0.02. These results meet the acceptance criteria for this test suite as developed in the FEHM VTP.

Table XVI. Results of the Heat Pipe Test			
V&V Test	Maximum Error	Maximum % Error	RMS Error
FE vs FDM flux at $t = 1*10^4$ days			
Vapor	1.044e-06	2.0170	8.950e-03
Liquid	2.028e-08	4.0070	1.071e-02

2.16 Test of Dry-Out of a Partially Saturated Medium

This test verifies that FEHM has correctly implemented the heat and mass transfer problem that combines water, water vapor, air, and heat transport. Figure 33 shows that the dry-out front computed using FEHM agrees closely with the analytical solution (results found in files dryout.analyt2-6) presented in the FEHM VTP for systems with and without vapor pressure lowering. The region of dried out rock proceeds as a sharp front with little spreading, and the rate of movement predicted by the code agrees well with the analytical solution. The maximum percent errors in the positions of the front(the position at which the saturation is 0.1, or dried to 50% of its initial value of 0.2) are 1.3% for both the vapor pressure lowering case and the case without vapor pressure lowering. Both of these errors are less than 5%, and thus these results meet the acceptance criteria for this test suite as developed in the FEHM VTP.

Table XVII. Results of the Dry-Out of a Partially Saturated Medium Test			
V&V Test	Maximum Error	Maximum % Error	RMS Error
Dryout Front vs. Time without Vapor Pressure Lowering			
Time 100 days	4.637e-05	0.1903	1.903e-03
Time 200 days	2.889e-04	0.5927	5.927e-03
Time 300 days	6.240e-04	0.8534	8.534e-03
Time 400 days	1.064e-03	1.0910	1.091e-02
Time 500 days	1.571e-03	1.2890	1.289e-02
Dryout Front vs. Time with Vapor Pressure Lowering			
Time 200 days	2.813e-04	1.1540	1.154e-02
Time 400 days	2.582e-04	0.5297	5.297e-03
Time 600 days	4.542e-05	6.212e-012	6.212e-04
Time 800 days	2.941e-04	0.3017	3.017e-03
Time 1000 days	7.099e-04	0.5826	5.826e-03
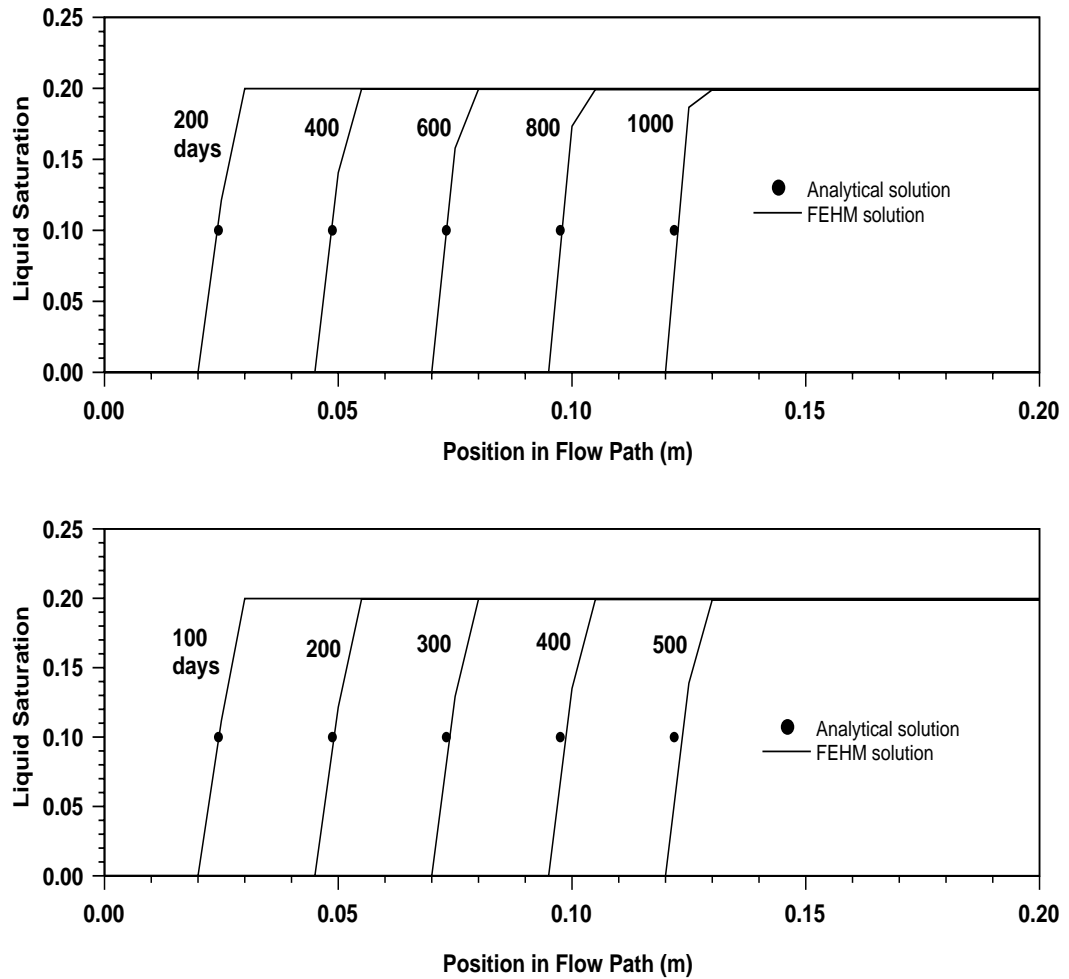
Figure 33. Comparison of FEHM and analytical solutions for the position of a dry-out front in a partially saturated medium. Cases with (top) and without (bottom) the effects of vapor pressure lowering are included.

2.17 Test of One Dimensional Reactive Solute Transport

This test verifies that FEHM has correctly implemented reactive tracer transport. Figures 34 to 38 show that FEHM results are in good agreement with the SORBEQ solutions. The results, compared numerically to the SORBEQ solutions (found in files sorbeq_out.cons, sorbeq_out.fr, sorbeq_out.lang. sorbeq_out.lin, and sorbeq_out.mfr) are given in Table XVIII. The maximum absolute error in concentration for the five isotherms was less than 0.03, the percent errors were less than 10%, and the RMS error was less than 0.01 when concentrations were greater than 0.1. These results meet the acceptance criteria for this test suite as developed in the FEHM VTP.

Table XVIII. Results of the Reactive Tracer Transport Test			
V&V Test	Maximum Error	Maximum % Error	RMS Error
Concentration vs. time at the outlet node (for C > 0.1)			
Conservative	9.711e-03	9.4930	2.902e-04
Linear	4.509e-03	2.2250	1.787e-04
Langmuir	9.151e-03	5.4050	2.385e-04
Freundlich	1.166e-02	2.1270	2.504e-04
Modified Freundlich	2.568e-02	8.0140	7.802e-04
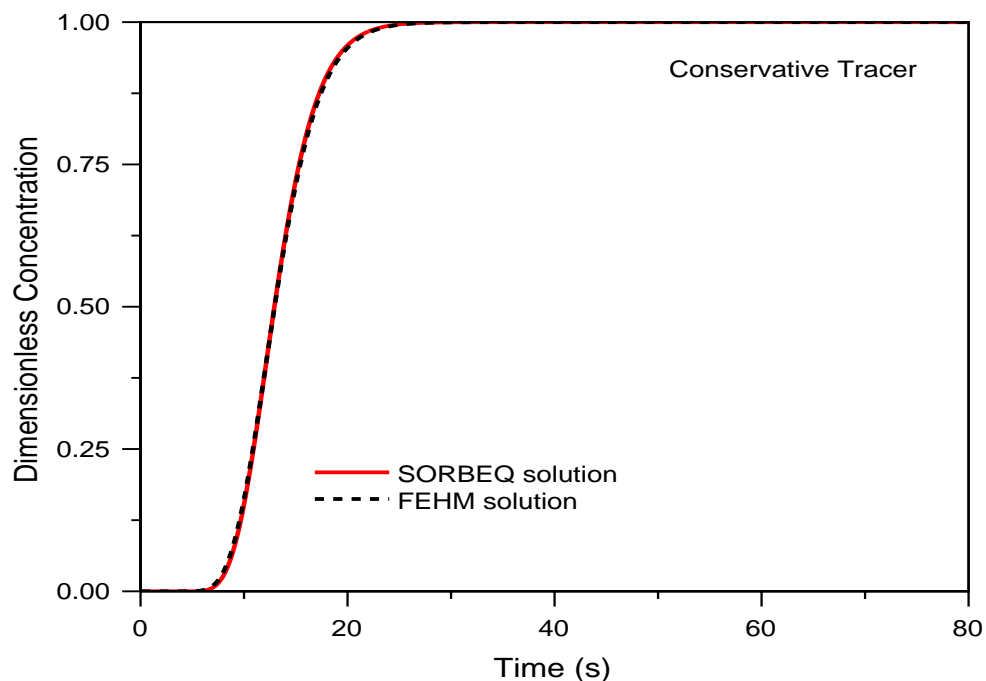
Figure 34. Comparison of FEHM and SORBEQ outlet concentrations for the conservative tracer.
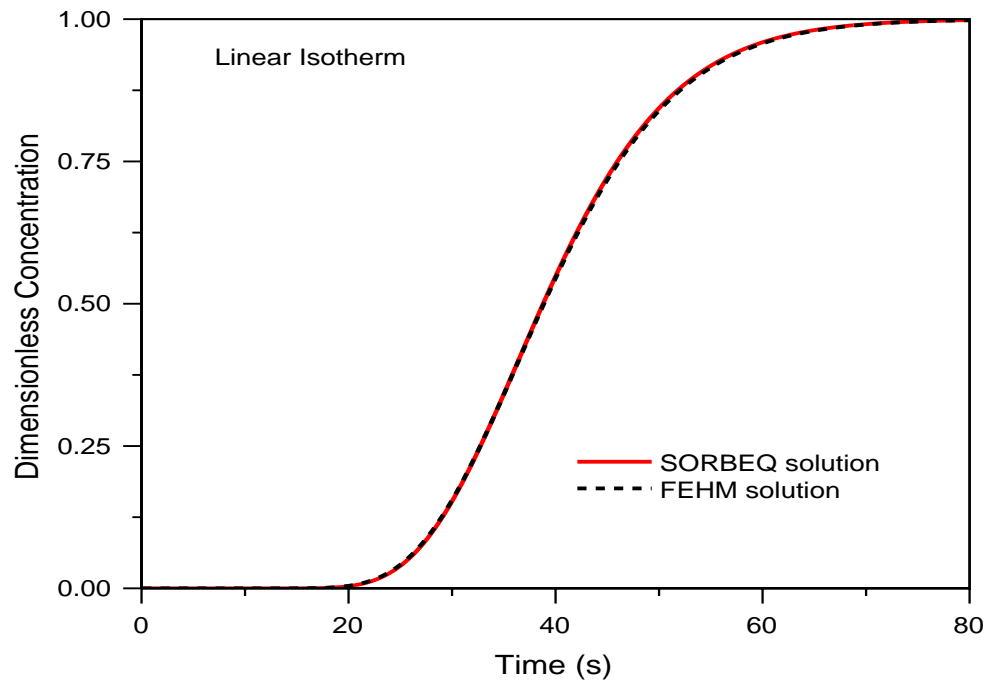
**Figure 35. Comparison of FEHM and SORBEQ outlet concentrations
for the linear isotherm.**
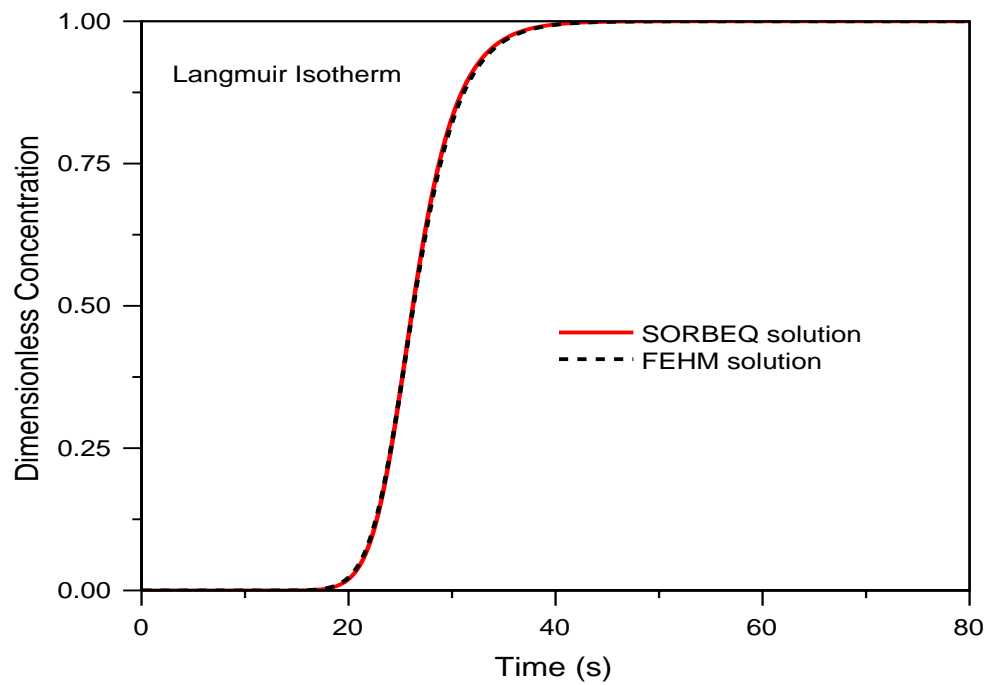
**Figure 36. Comparison of FEHM and SORBEQ outlet concentrations
for the Langmuir isotherm.**
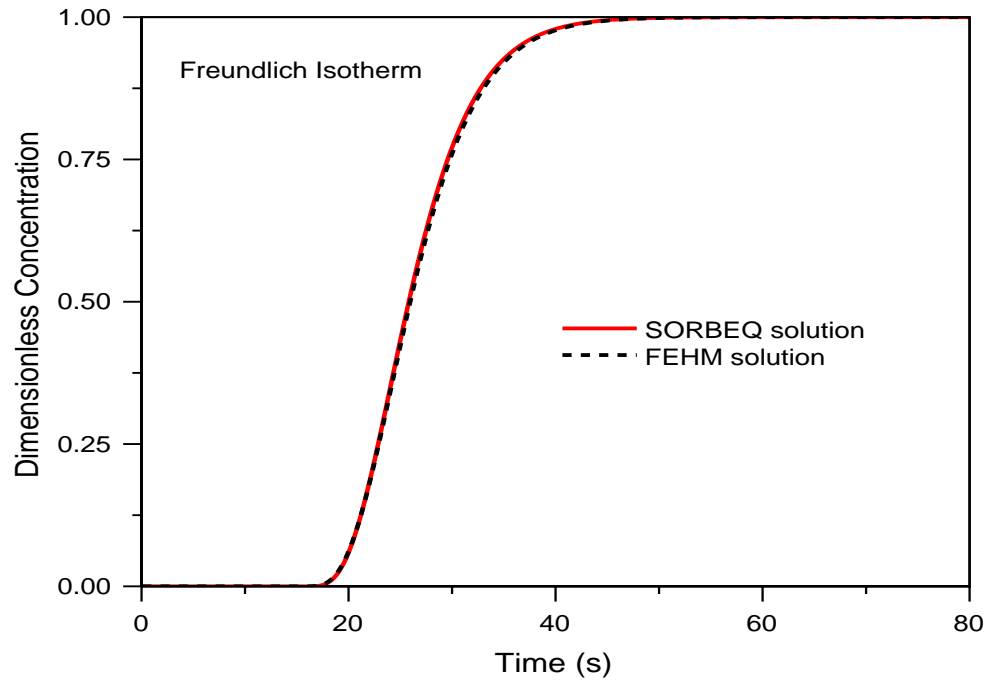
Figure 37. Comparison of FEHM and SORBEQ outlet concentrations for the Freundlich isotherm.
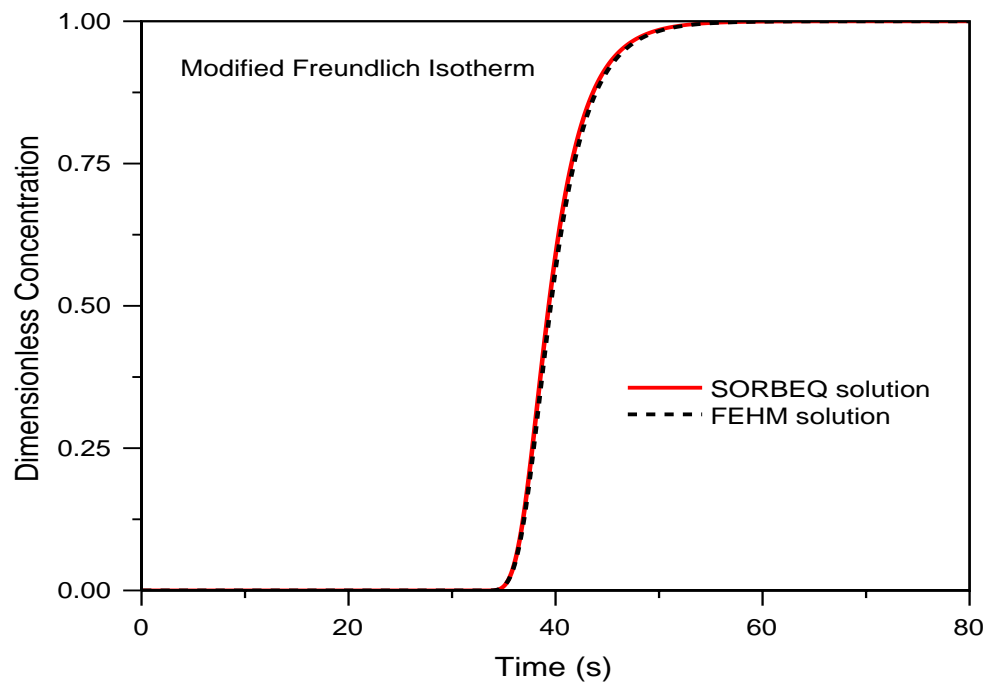
Figure 38. Comparison of FEHM and SORBEQ outlet concentrations for the modified Freundlich isotherm.

2.18 Test of Henry's Law Species

2.18.1 Air Movement Through Stagnant Water

This test verifies that FEHM has correctly implemented Henry's law solutes for air moving through a stagnant fluid phase. Figure 39 shows that FEHM results are in good agreement with the analytical solution. The results, compared numerically to the analytical solution (found in file henry1_out.analyt) are given in Table XIX. The maximum absolute error for Test 1 was less than 0.01, and the RMS error was less than 0.01 for concentrations greater than 0.1. These results meet the acceptance criteria for this test suite as developed in the FEHM VTP.

Table XIX. Results of the Henry's Law Species Test			
V&V Test	Maximum Error	Maximum % Error	RMS Error
Concentration vs. time at the outlet node (for C > 0.1)			
Mobile air phase	9.947e-03	7.4640	4.910e-04
Mobile water phase	7.292e-03	2.7220	2.904e-04
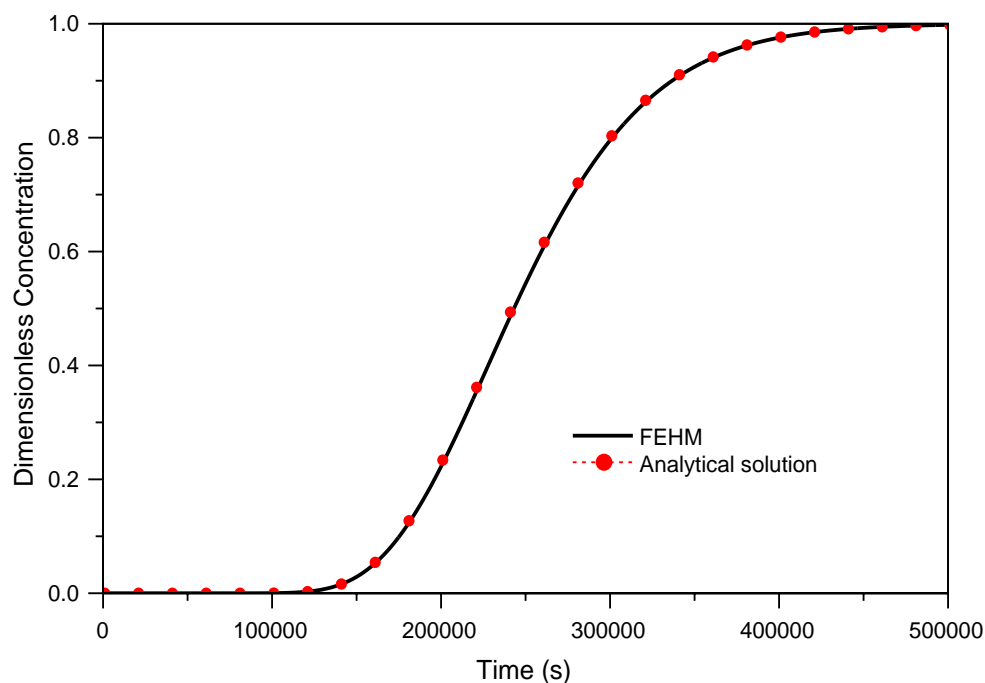
Figure 39.Comparison of FEHM results with the analytical solution for a mobile air phase.

2.18.2 Water Movement Through Stagnant Air

This test verifies that FEHM has correctly implemented Henry's law solutes for water moving through a stagnant air phase. Figure 40 shows that FEHM results are in good agreement with the analytical solution. The results, compared numerically to the analytical solution (found in file henry2_out.analyt) are given in Table XIX. The maximum absolute error

for Test 2 was less than 0.0073, and the RMS error was less than 0.01 when concentrations were greater than 0.1. These results meet the acceptance criteria for this test suite as developed in the FEHM VTP.
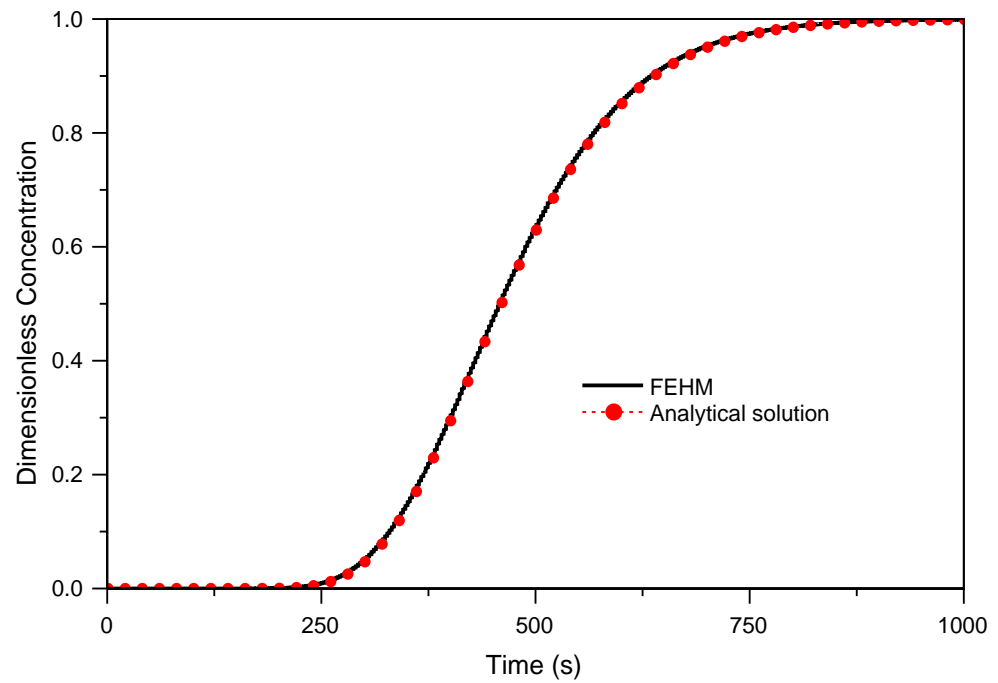
Figure 40.Comparison of FEHM results with the analytical solution for a mobile water phase.

2.19 Test of Fracture Transport With Matrix Diffusion

This test verifies that FEHM has correctly implemented the solute transport
solution with equilibrium sorption in two dimensions and for the Generalized
Dual Porosity (GDPM) code option. Figure 41 shows that FEHM's numerical
solution is in good agreement with the analytical solution of Tang et al. (1981) for
test cases that include matrix diffusion with no sorption, sorption in the matrix,
and sorption on the fracture surfaces and in the matrix. It also illustrates that
there is no discernible difference between results when the GDPM option is used.
The slight discrepancies are probably due to numerical errors associated with
insufficiently small grid spacings adjacent to the fracture. This would render the
solution inaccurate at early times in the simulation, when concentration
gradients near the fracture are largest. Nonetheless, the agreement is almost
certainly adequate for any analysis that would be made using these model
results. The results, compared numerically to the analytical solution (found in
files tang1.analyt, tang2.analyt, and tang3.analyt) are given in Table XX. The
maximum absolute error for these runs was less than 0.032, and the maximum
percent errors ranged from 4.7 - 19.1% for concentration values greater than 0.1.
The RMS error ranged from 0.0014 to 0.0027. These results meet the acceptance
criteria for this test suite as developed in the FEHM VTP.

Table XX. Results of the Fracture Transport/Matrix Diffusion Test			
V&V Test	Maximum Error	Maximum % Error	RMS Error
Concentration vs. time at the outlet node (for C > 0.1)			
No sorption	2.810e-02	9.0940	1.412e-03
Matrix sorption	1.759e-02	13.3800	2.205e-03
Fracture and matrix sorption	1.707e-02	4.6620	2.108e-03
Concentration vs. time at the outlet node - GDPM formulation (for C > 0.1)			
No sorption	3.135e-02	11.7800	1.577e-03
Matrix sorption	2.363e-02	19.1300	2.670e-03
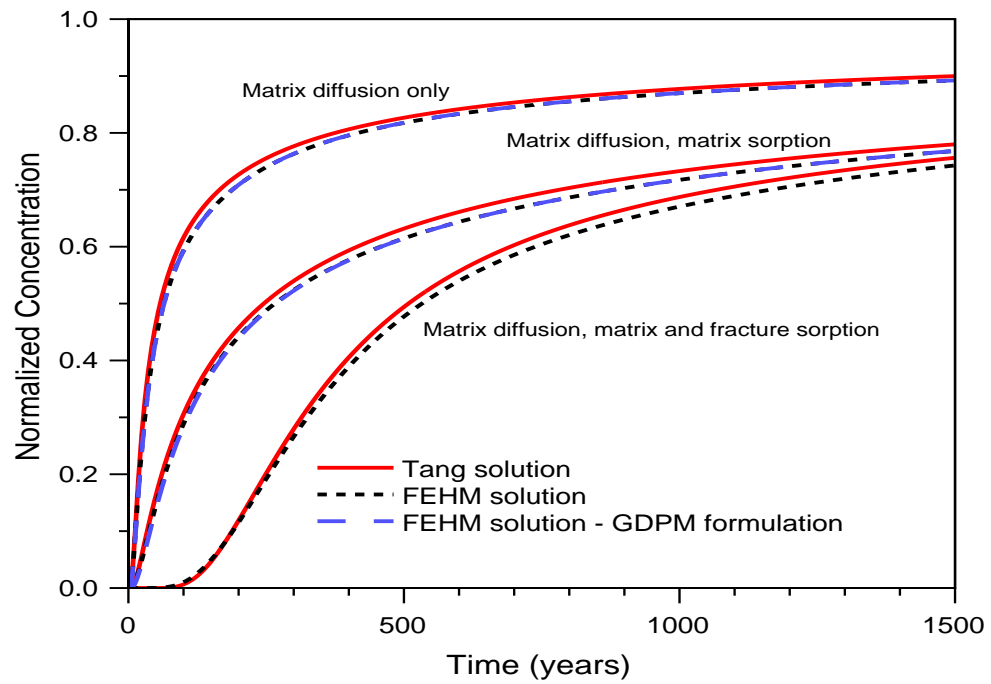
Figure 41. Comparison of FEHM and Tang analytical solutions for concentration versus time for the matrix diffusion model.

2.20 Test of the Movement of a Dissolved Mineral Front

This test verifies that FEHM has correctly implemented the reactive transport system consisting of one-dimensional transport with the movement of a dissolved mineral front. Figure 42 compares the front location and shape simulated using FEHM to that predicted from the analytical solution. The results agree closely, with FEHM's numerical results exhibiting a very slight spreading of the dissolution front. Nonetheless, the position of the front agrees with the predicted value (found in files dissolution.analyt2, dissolution.analyt3, and dissolution.analyt4) to within a maximum error of 3.2%. This error is less than 5% and these results meet the acceptance criteria for this test suite as developed in the FEHM VTP. It should be noted for this problem the RMS error is a single point average for each time.

Table XXI. Results of the Movement of a Dissolved Mineral Front Test			
V&V Test	Maximum Error	Maximum % Error	RMS Error
Dissolution Front vs. Time			
Time 20000. s	2.161e-03	3.2250	3.225e-02
Time 60000. s	3.323e-03	1.6530	1.653e-02
Time 100000. s	6.281e-04	0.1875	1.875e-03
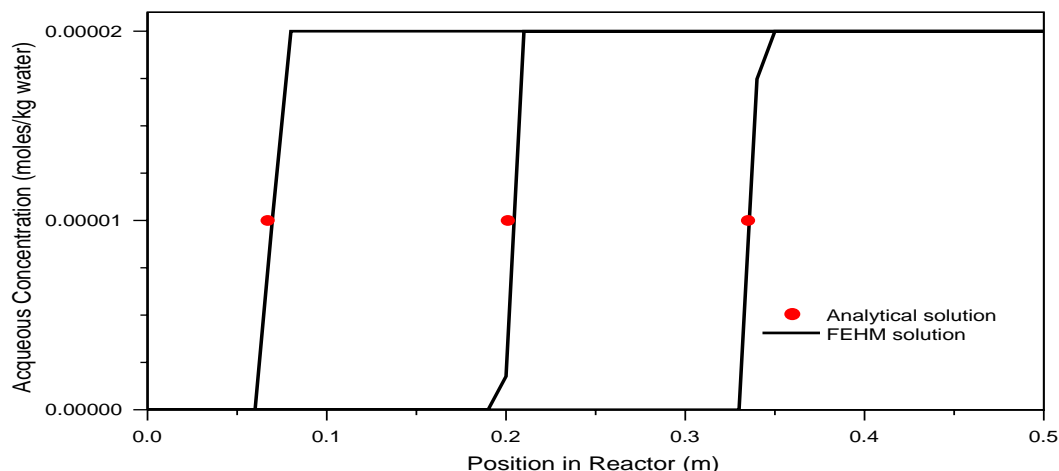
Figure 42. Comparison of FEHM and the analytical solution for the position of the dissolved mineral front at the final time of the simulation.

2.21 Test of Multi-Solute Transport with Chemical Reaction

This test verifies that FEHM has correctly implemented the transport of multiple, chemically interacting species in solution for a mixed kinetic and equilibrium reaction system. Figure 43 compares the breakthrough curves for aqueous species for FEHM and PDREACT, the code used for the comparison. Figure 44 compares the solid concentrations versus time at the outlet of the system for the two codes. There is excellent agreement between the two codes for this reactive transport problem. The PDREACT ouput is found in files multi.pdreact_CoEDTA_aq.out, multi.pdreact_CoEDTA_s.out, multi.pdreact_Co_aq.out, multi.pdreact_Co_s.out, multi.pdreact_EDTA_aq.out, multi.pdreact_FeEDTA_aq.out, multi.pdreact_FeEDTA_s.out, and multi.pdreact_Fe_aq.out. Table XXII indicates that the percent errors of all species at the outlet were less than 6% for concentrations greater than 10% of their peak values. These results meet the acceptance criteria for this test suite as developed in the FEHM VTP. Numerical results for aqueous $EDTA$ and Fe are not considered because the concentrations are very near zero, and at such low concentrations, a good measure of error is not available.

Table XXII. Results of Multi-Solute Reactive Transport Test			
V&V Test	Maximum Error	Maximum % Error	RMS Error
Aqueous Species Concentration vs. Time (for $C > 0.1\ C_{peak}$)			
Co	3.916e-06	0.7115	3.879e-04
$CoEDTA$	1.442e-04	3.6850	2.222e-03
$FeEDTA$	3.667e-05	2.6400	1.747e-03
Solid Species Concentration vs. Time (for $C > 0.1\ C_{peak}$)			
Co	1.866e-05	0.9680	6.416e-04
$CoEDTA$	7.826e-05	5.8390	3.178e-03
$FeEDTA$	1.438e-05	3.2470	2.229e-03
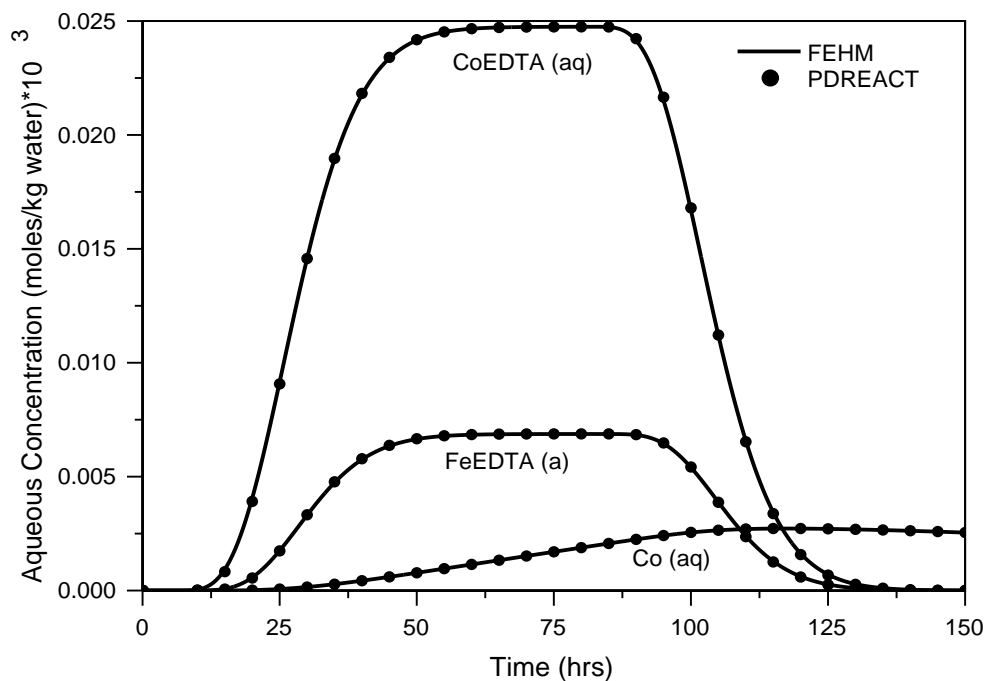
Figure 43. Comparison of FEHM and PDREACT for the breakthrough curves of aqueous species.
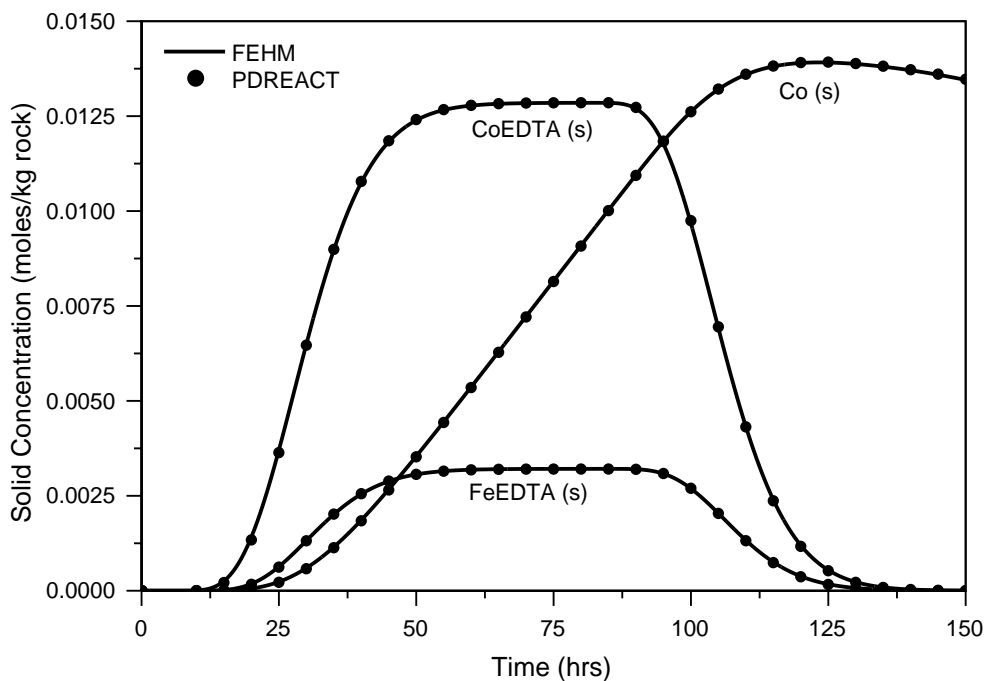
Figure 44. Comparison of FEHM and PDREACT for the exit concentration versus time for solid species.

2.22 Test of Three-Dimensional Radionuclide Transport with Decay Chain

This test verifies that FEHM has correctly implemented the transport module when used to simulate a radionuclide decay chain transport problem in three dimensions. Figures 45, 46, 47, and 48 compare the concentration-time curves for the radionuclide and conservative tracer simulated using FEHM and TRACRN, the code used for comparison, at four different positions. Regarding the code comparison, the plots indicate that FEHM and TRACRN concentrations agree quite closely at the comparison points. Results from TRACRN are found in files 3d_tracr3d_cons.out and 3d_tracr3d_am.out. Considerable concentration errors can result from only a small displacement of a breakthrough curve along the time axis because of the steep rise or fall of the concentration-time curve for a typical case as seen by the maximum percent errors which varied from 3 - 15 %. However, Table XXIII indicates that the RMS errors of all species at each comparison point were less than 0.005 (or 0.5 %) for concentrations greater than 10% of their peak values. These results meet the acceptance criteria for this test suite as developed in the FEHM VTP.

Table XXIII. Results of Three-Dimensional Decay Chain Test Problem			
V&V Test	Maximum Error	Maximum % Error	RMS Error
Conservative Tracer Concentration vs. Time (for $C > 0.1\ C_{peak}$)			
Point 1	5.297e-02	6.6030	1.308e-03
Point 2	1.607e-02	10.7800	1.812e-03
Point 3	3.639e-03	4.5220	8.517e-04
Point 4	1.004e-03	2.8120	1.244e-03
^{243}Am Concentration vs. Time (for $C > 0.1\ C_{peak}$)			
Point 1	4.800e-02	7.2750	1.523e-03
Point 2	1.589e-02	14.8100	3.423e-03
Point 3	1.041e-03	12.6800	3.289e-03
Point 4	1.983e-05	14.9700	4.213e-03
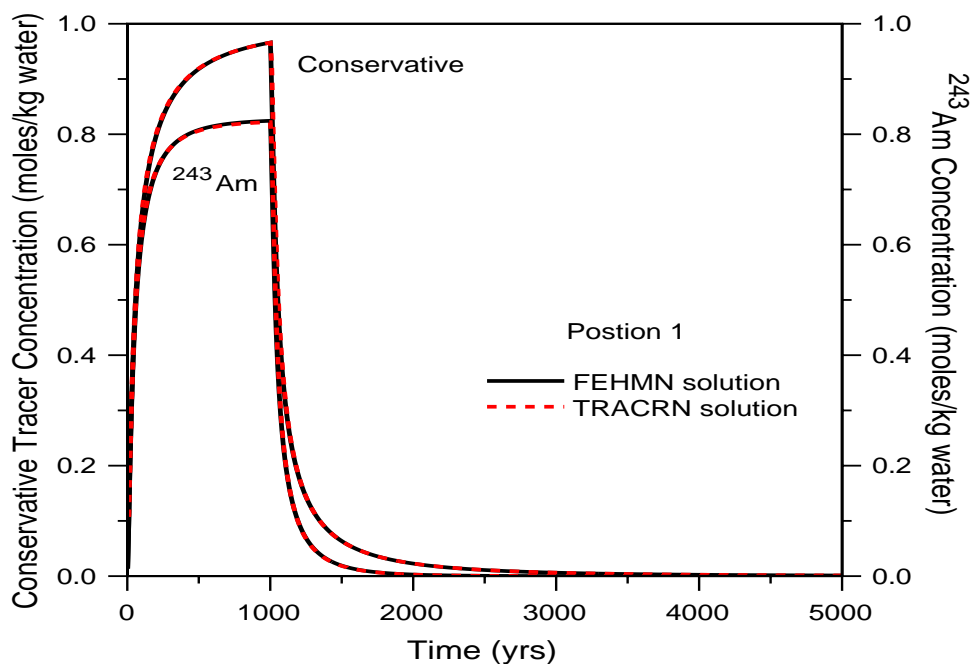
Figure 45. Comparison of FEHM and TRACRN results for the concentration-time history at position 1.
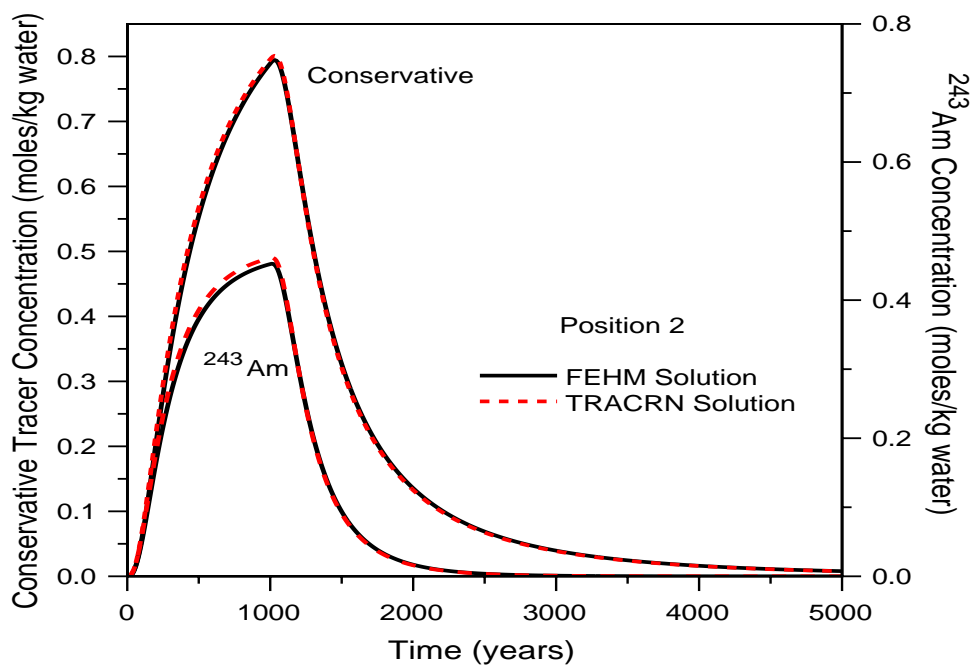
Figure 46. Comparison of FEHM and TRACRN results for the concentration-time history at position 2.
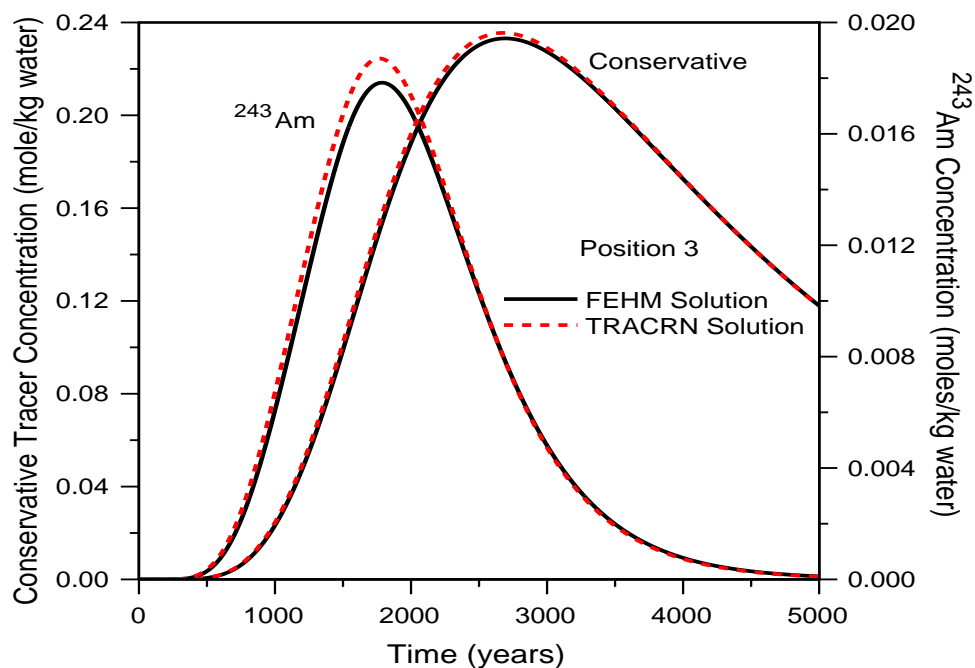
**Figure 47. Comparison of FEHM and TRACRN results for the
concentration-time history at position 3.**
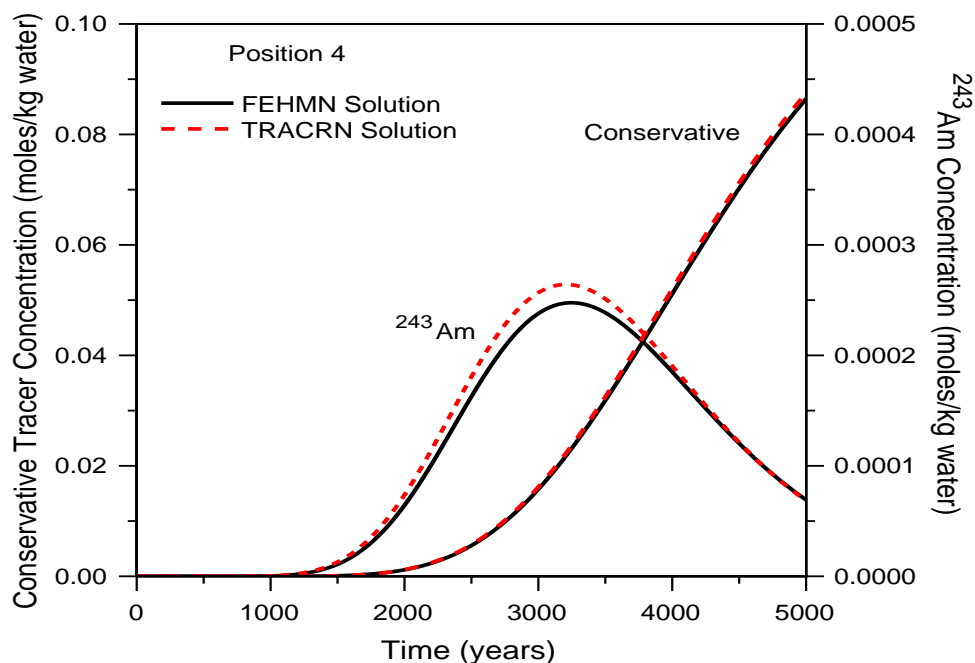
**Figure 48. Comparison of FEHM and TRACRN results for the
concentration-time history at position 4.**

2.23 Test of Streamline Particle Tracking Model

2.23.1 Breakthrough Curve and In Situ Concentration Profile Tests

This test verifies that FEHM has correctly implemented the streamline particle-tracking module when used to simulate longitudinal dispersion with and without sorption and matrix diffusion, and in situ concentrations assuming longitudinal and transverse dispersion. Figures 49 and 50 compare the breakthrough concentration-time curves with and without matrix diffusion and sorption. Figure 51 compares the in situ concentration profiles, and as anticipated, shows how increasing the number of particles improves the FEHM solution. Regarding the code comparison, the plots indicate that FEHM, 3DADE, and Tang concentrations agree quite closely. Results from 3DADE are found in files sptr1.analyt, sptr2.analyt, plume_4800.analyt, and plume_10000.analyt. Results for the Tang solution are found in file sptr3.analyt. Considerable concentration errors can result from only a small displacement of a breakthrough curve along the time axis because of the steep rise or fall of the concentration-time curve for a typical case as seen by the maximum percent errors which varied from 20 - 35%. However, Table XXIV indicates that the RMS errors for each breakthrough test were less than 0.004 for concentrations greater than 10% of their peak values. Maximum percent errors for the in situ concentration profile comparisons ranged from 3 - 16 %, while RMS errors were less than 0.03 for concentrations greater than 5% of their peak values. These results meet the acceptance criteria for this test suite as developed in theFEHM VTP.

Table XXIV.Results of Streamline Particle Tracking Model for the Breakthrough Curve and In Situ Concentration ProfileTest Problems

V&V Test	Maximum Error	Maximum % Error	RMS Error
Breakthrough Concentration (15 km from inlet) vs. Time (for $C > 0.1\ C_{peak}$)			
No Sorption	5.882e-02	34.6100	1.755e-03
Matrix Sorption	5.494e-02	31.6200	3.589e-03
Matrix Diffusion, No Sorption	4.368e-02	19.9400	3.680e-03
Concentration Profile at X = 5000 m (for $C > 0.05\ C_{peak}$)			
10,000 Particles	2.252e-02	15.6300	2.770e-02
100,000 Particles	5.873-e03	10.9400	1.820e-02
Concentration Profile at X = 10000 m (for $C > 0.05\ C_{peak}$)			
10,000 Particles	1.151e-02	14.0200	2.369e-02
100,000 Particles	8.088e-03	3.8860	7.793e-03
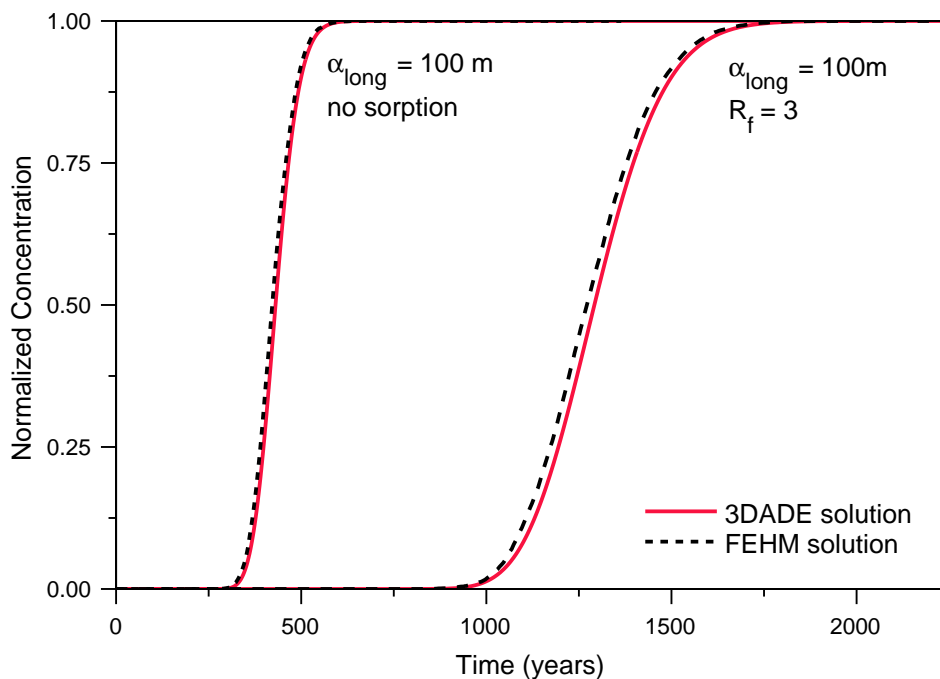
Figure 49. Comparison of FEHM and 3DADE results for concentration versus time at a position 15 km from inlet.
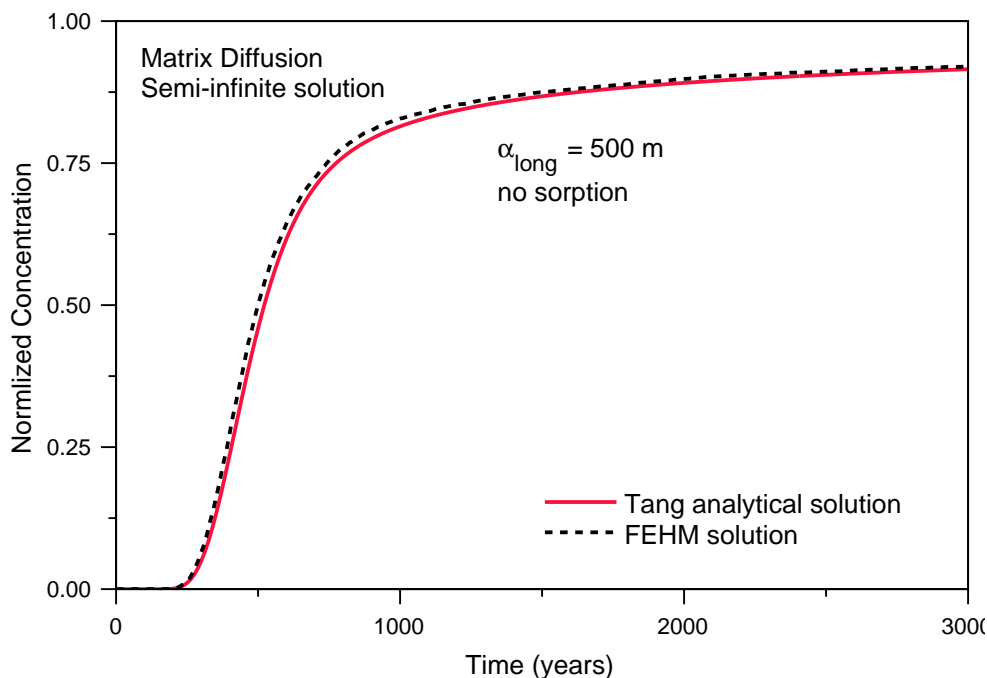
Figure 50. Comparison of FEHM and Tang analytical results for concentration versus time at a position 15 km from inlet..
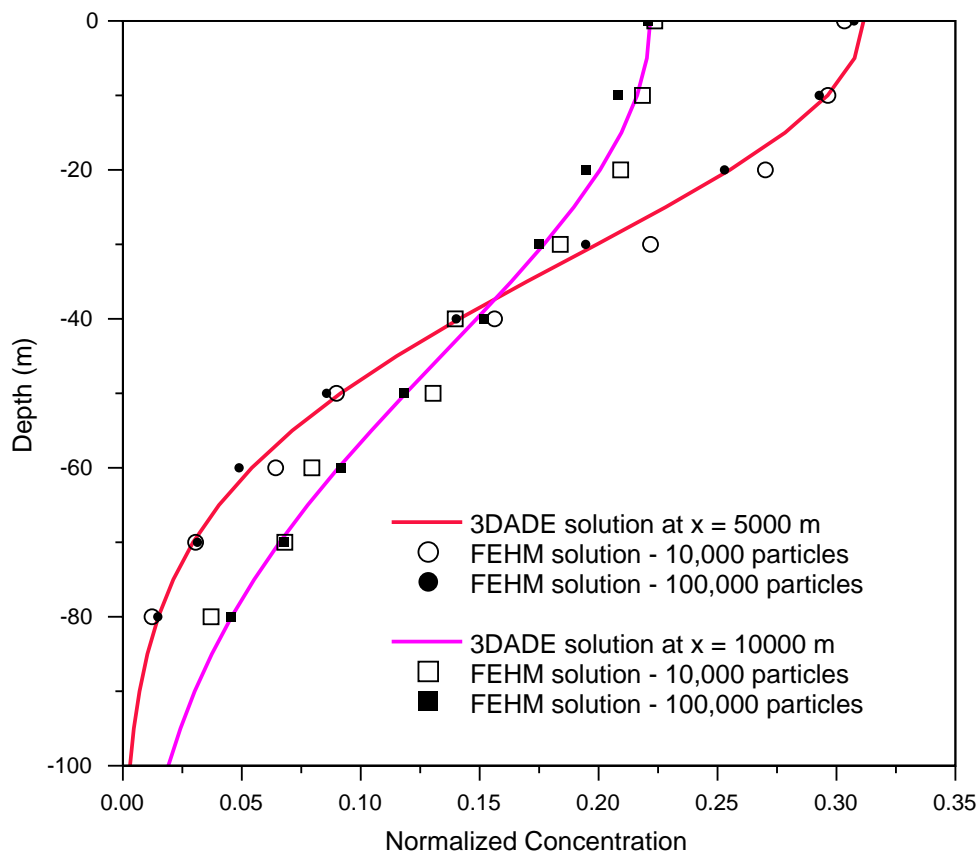
Figure 51. Comparison of FEHM and 3DADE results for concentration profiles at x = 5000 m and x = 10000 m.

2.23.2 Test of the Generalized Dispersion Tensor

Table XXV shows that the generalized dispersion tensor has also been correctly implemented. Standard deviation calculated from FEHM particle locations, when compared to the theoretical values are within 2 %, and results meet the acceptance criteria for this test suite as developed in the FEHM VTP.

Table XXV. Comparison of Standard Deviation at 6.949*10^8 daysfor the Generalized Dispersion Tensor Test Problem						
Case	Δx (m)		Δy (m)		Δz (m)	
	Theory	FEHM	Theory	FEHM	Theory	FEHM
Burnett and Frind	147	145.5	88	87.6	147	146.1
Error	1.020 %		0.455 %		0.612 %	
Modified Burnett and Frind	133	133.8	118	115.7	133	133.2
Error	0.602 %		1.949 %		0.150 %	
Generalized Axisymetric	516	516.3	329	328.9	140	139.2
Error	0.058 %		0.030 %		0.571 %	

2.23.3 Test of Reverse Tracking Model

This test verifies that FEHM has correctly implemented reverse particle tracking within the streamline particle tracking module. Figure 52 shows the tracks obtained for the forward and reverse simulations. In the figure, the solid symbols represent the forward tracks while the reverse tracks are plotted with open symbols. Table XXVI indicates the maximum distance between particle locations on the forward and reverse tracks was less than 1m for this test and the results meet the acceptance criteria for this test suite as developed in the FEHM VTP.
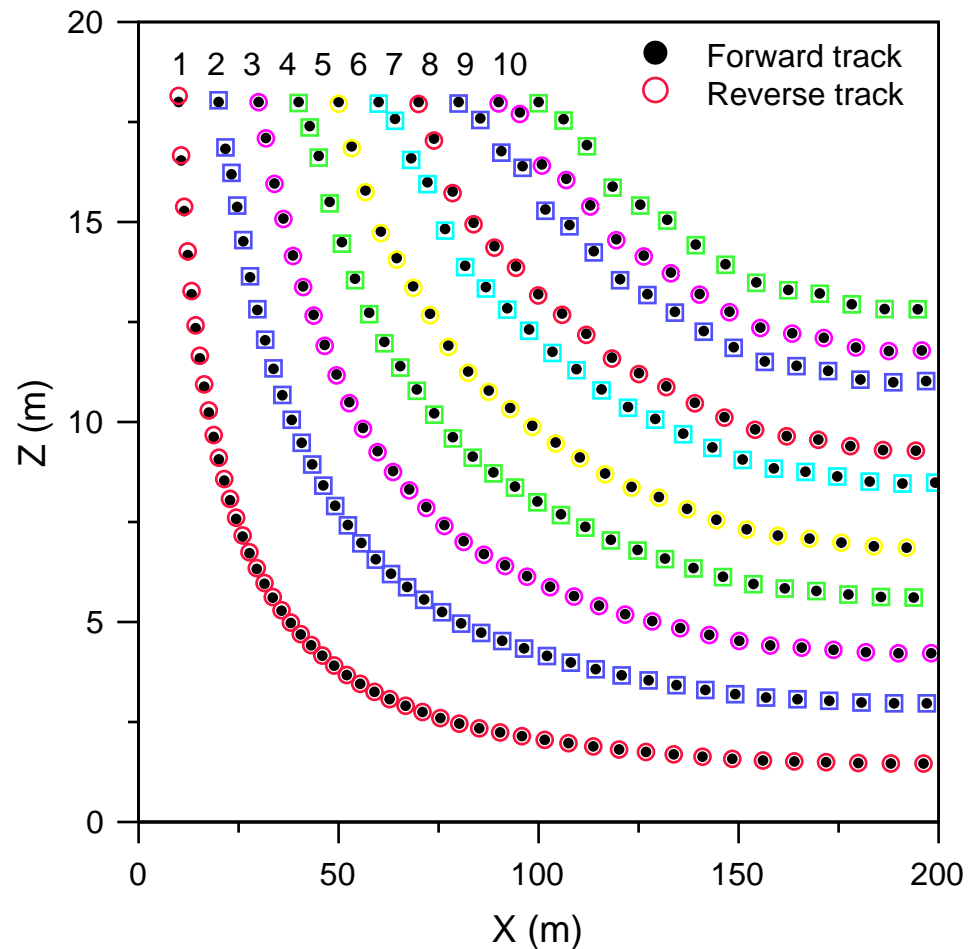
Figure 52. Comparison of FEHM forward and reverse track particle positions.

Table XXVI. Results of Streamline Particle Tracking Model for the Reverse Tracking Test Problem	
Particle Number	Maximum Distance (m)
1	0.1525
2	0.0432
3	0.0282
4	0.0421
5	0.0477
6	0.0498
7	0.0503
8	0.0430
9	0.0413
10	0.0326

2.23.4 Test of Particle Capture Model

This test verifies that FEHM has correctly implemented particle capture near pumping nodes within the streamline particle tracking module. Figure 53 shows the particle tracks obtained using the coarse and fine meshes with a pumping node in the center. Figure 54 shows a closer view of the tracks within 100 m of the pumping node. The black circles represent the coarse grid particle positions, while the fine grid particle positions are shown in red. Visual inspection shows a close simillarity between the tracks, with differences being difficult to discern in Figure 54. The results are compared numerically in Table XXVII which reports the maxium and average distances between particle locations for the two meshes. The differences are also given as a percent of the coarse grid spacing.

Table XXVII indicates the maximum distance between particle locations was 16.866 m or 10.063 % of the coarse grid spacing. These results meet the acceptance criteria for this test suite as developed in the FEHM VTP.

Table XXVII. Results of Streamline Particle Tracking Model for the Particle Capture Model Test Problem				
Particle Number	Maximum Distance (m)	% of Coarse Grid Spacing	Average Distance (m)	% of Coarse Grid Spacing
1	4.5784	2.7317	1.6858	1.0058
2	5.3139	3.1706	2.7453	1.6380
3	16.866	10.0630	8.7155	5.2002
4	7.1186	4.2474	2.8883	1.7233
5	10.060	6.0023	0.7526	0.4491
6	2.9611	1.7668	0.4136	0.2468
7	3.0499	1.8198	0.4273	0.2550
8	13.840	8.2576	0.8486	0.5063
9	5.1977	3.1012	2.9339	1.7505
10	15.389	9.1820	7.8195	4.6656
11	7.3289	4.3729	3.6090	2.1533
12	5.9669	3.5602	2.3118	1.3793
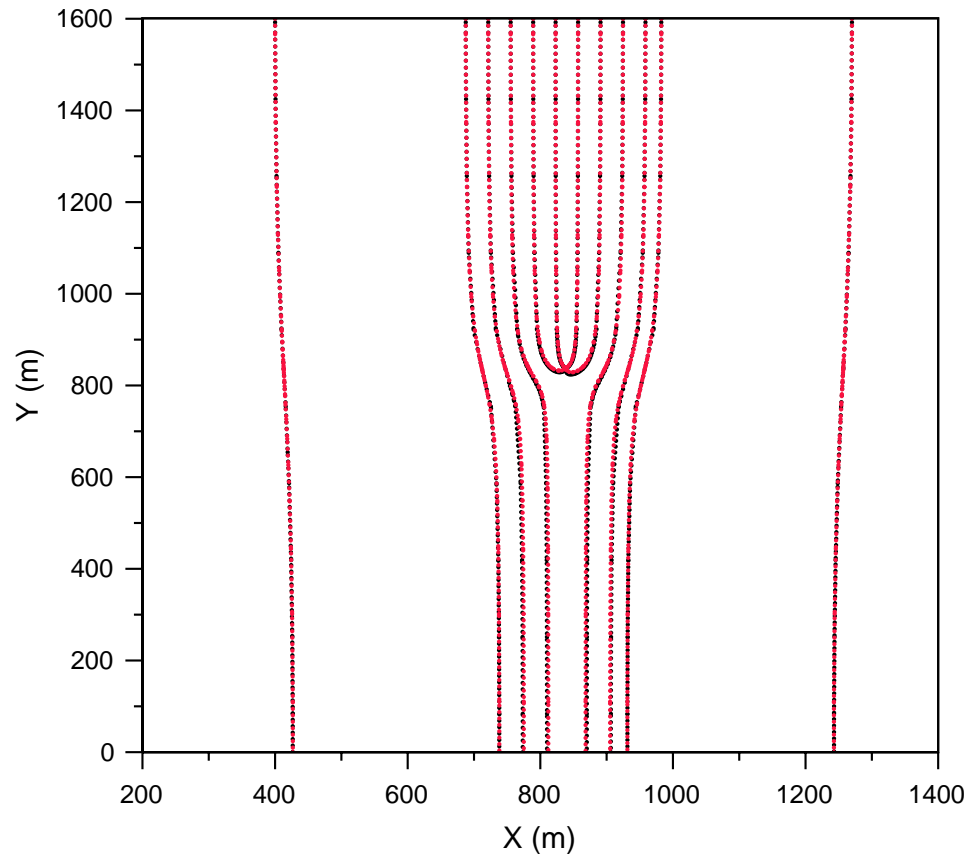
Figure 53. Comparison of particle tracks for the particle capture model using a coarse and fine grid.

2.23.5 Test of Divergence of Dispersion Tensor Model

This test verifies that FEHM has correctly implemented random walk particle transport and tests the divergence of the dispersion tensor model. Figure 55 shows the particle tracks obtained using the coarse and fine meshes. The black dots represent the coarse grid particle positions, while the fine grid particle positions are shown in red. The results are compared numerically in Table XXVIII which reports the maxium and average distances between particle locations for the two meshes. The differences are also given as a percent of the coarse grid spacing. Table XXVIII indicates the maximum distance between particle locations was 31.25 m. These results meet the acceptance criteria for this test suite as developed in the FEHM VTP.

Table XXVIII. Results of Streamline Particle Tracking Model for the Divergence of Dispersion Tensor Model Test Problem		
Particle Number	Maximum Distance (m)	Average Distance (m)
1	31.2474	13.1652
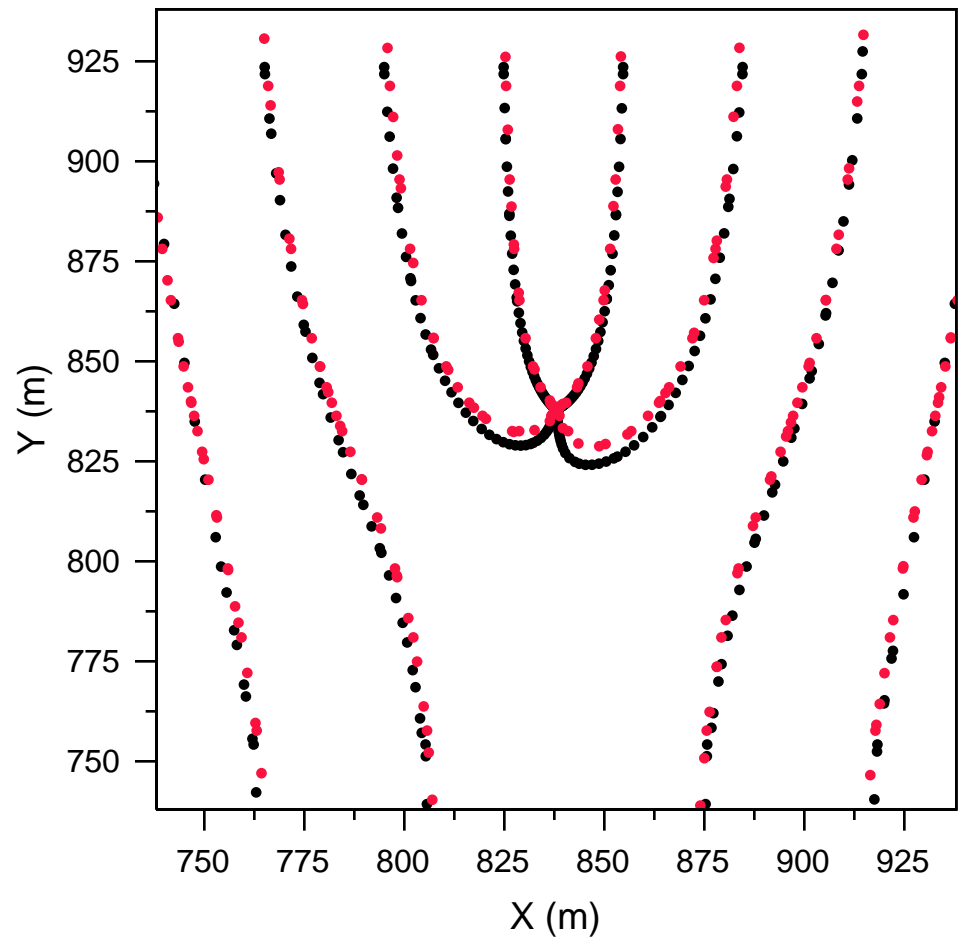
Figure 54. Comparison of particle tracks for the particle capture model near the pumping node using a coarse and fine grid.
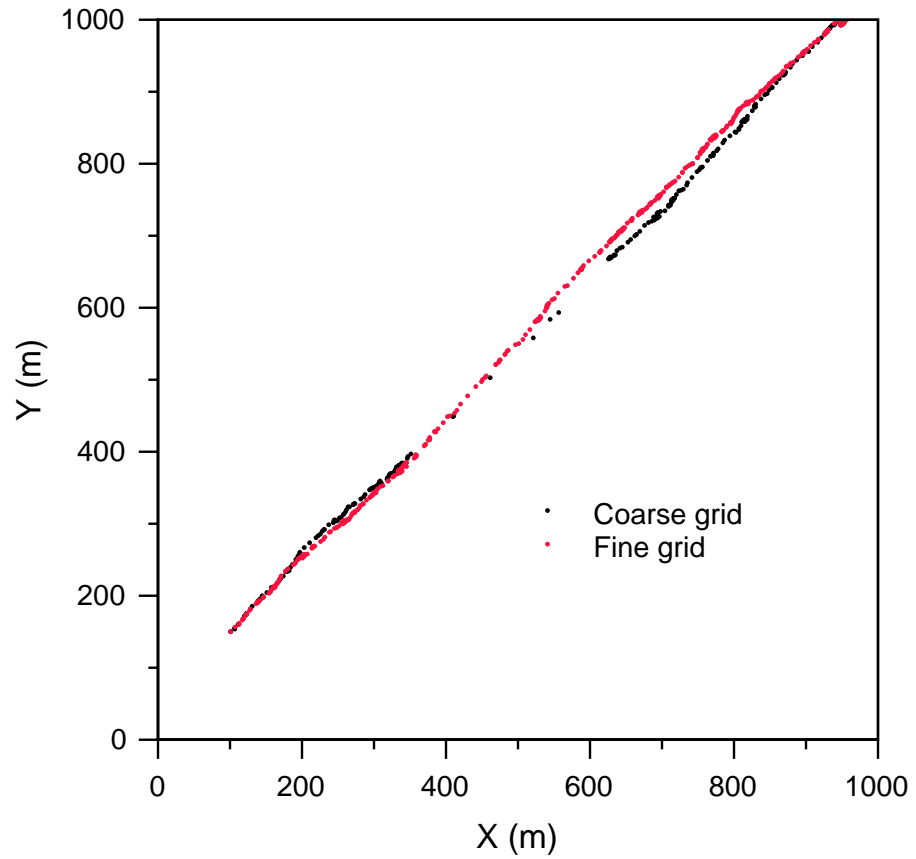
Figure 55. Comparison of particle tracks for the test of divergence of dispersion tensor model using a coarse and fine grid.

2.24 Test of Cell-Based Particle Tracking Model

This test verifies that FEHM has correctly implemented the cell-based particle tracking model when used to simulate breakthrough curves of longitudinal dispersion with and without sorption and matrix diffusion. It also verifies that the decay-chain option of the multiple-species particle-tracking model properly accounts for radioactive decay chains for a mixed case of conservative and sorbing radionuclides. Figures 56, 57, and 58, compare the breakthrough concentration-time curves for the FEHM numerical and Tang analytical solutions. Figure 59 compares the breakthrough concentration-time curves for the radionuclide decay chain simulated using FEHM and CHAIN, the code used for comparison. Results for the Tang analytical solution are found in files tang_ptrk1.analyt, tang_ptrk2.analyt, and tang_ptrk3.analyt. Results for the CHAIN decay-chain solution are found in files chain1.analyt, chain2.analyt, chain3.analyt, and chain4.analyt. Considerable concentration errors can result from only a small displacement of a breakthrough curve along the time axis because of the steep rise or fall of the concentration-time curve for a typical case as seen by the maximum percent errors which varied from 3 - 49 %. However, Table XXIX indicates that the RMS errors were less than 0.01 (or 1.0 %) for concentrations greater than 10% of their peak values for the single species tests, and less than 0.04 (or 4.0 %) for concentrations greater than 10% of their peak values for the decay-chain test. These results meet the acceptance criteria for this test suite as developed in the FEHM VTP.

Table XXIX.Results of Cell-Based Particle Tracking Model Test Problems			
V&V Test	Maximum Error	Maximum % Error	RMS Error
Breakthrough Concentration vs. Time (for $C > 0.1\ C_{peak}$)			
No Sorption	3.948e-02	10.9800	7.055e-03
Matrix Sorption	4.073e-02	9.4990	6.158e-03
Matrix Diffusion, Matrix & Fracture Sorption	8.149e-03	3.3540	6.223e-04
Breakthrough Concentration (number of particles) vs. Time for the Decay-Chain Test (for $C > 0.1\ C_{peak}$)			
Species 1	819.3000	41.9800	3.499e-02
Species 2	234.6000	36.8500	2.939e-02
Species 3	128.0000	19.8100	1.145e-02
Species 4	130.3000	48.9100	3.719e-02

Values for the cumulative breakthrough with time of the four species from GoldSim have been plotted and compared visually to the results of the radioactive decay chain test case (Figure 60). There are no systematic differences between the GoldSim output and the results of FEHM. These results meet the acceptance criteria for this test suite as developed in the FEHM VTP.

For the dual permeability test cases, visual comparisons are applied to ensure that the code is functioning properly and to examine the limits of applicability of the model. The first comparison, shown in Figure 61, is for the case of flow only in the fracture, with the two-parameter transfer function curves of the Sudicky and Frind (1982) model used. Both the conservative and sorbing tracer
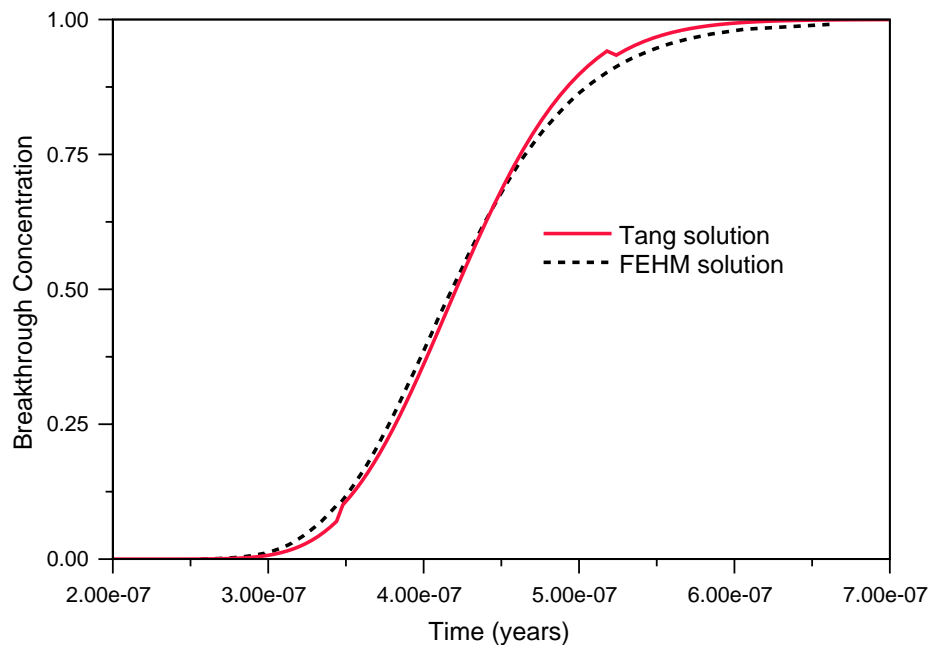
Figure 56. Comparison of FEHM and Tang analytical solutions for breakthrough concentration versus time for the conservative (no sorption) model.
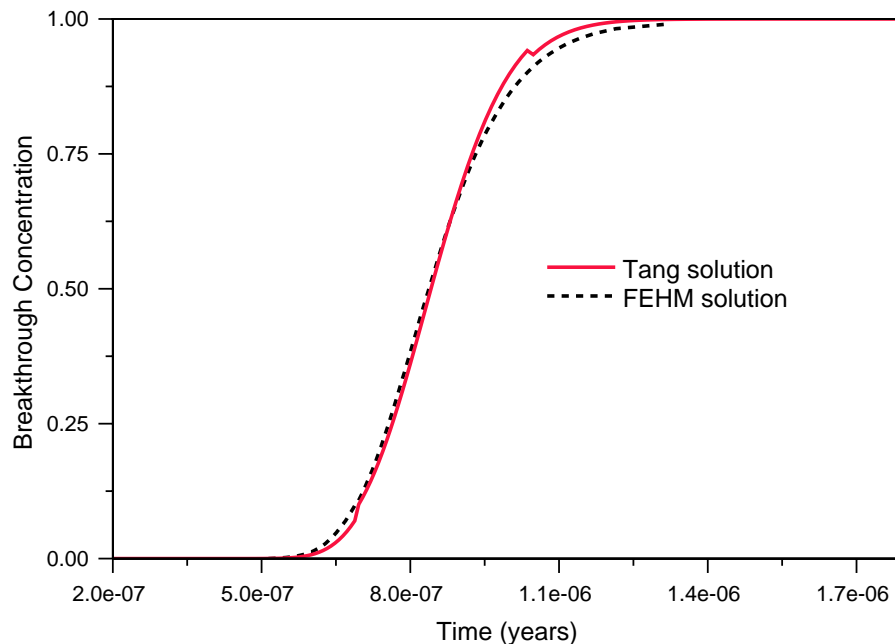
Figure 57. Comparison of FEHM and Tang analytical solutions for breakthrough concentration versus time for the sorbing model.
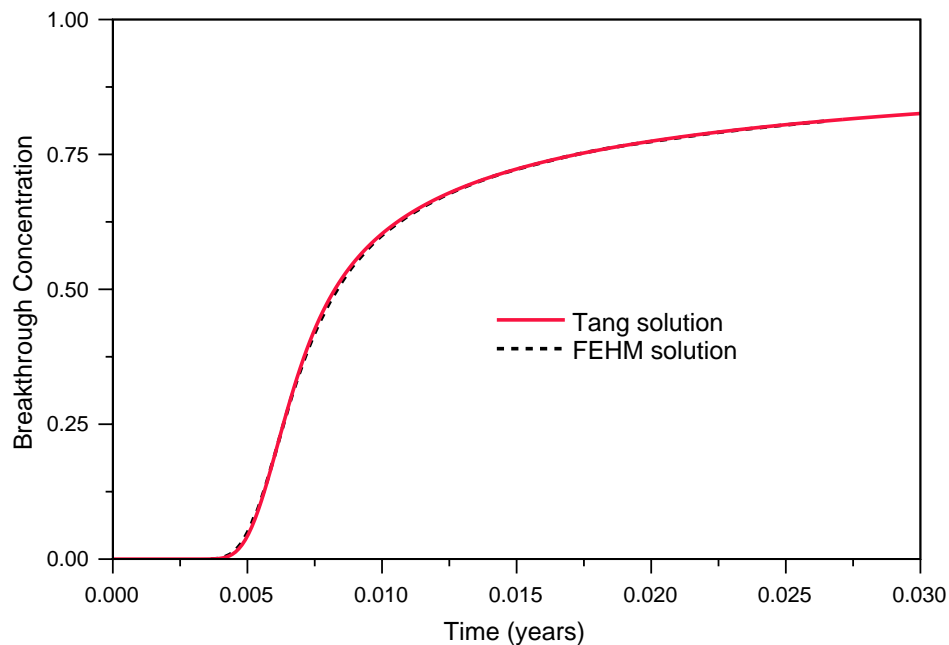
Figure 58. Comparison of FEHM and Tang analytical solutions for breakthrough concentration versus time for the matrix diffusion with sorption model.

Figure 59. Comparison of FEHM and CHAIN solutions for breakthrough concentration versus time for the decay-chain test.

Figure 60. Comparison of GoldSim and FEHM solutions for cumulative breakthrough concentration versus time for the decay-chain test.

breakthrough curves are matched very closely using the algorithm that assumes a regular spacing of transfer function parameters. Two other interpolation schemes are also shown in the figure for the conservative tra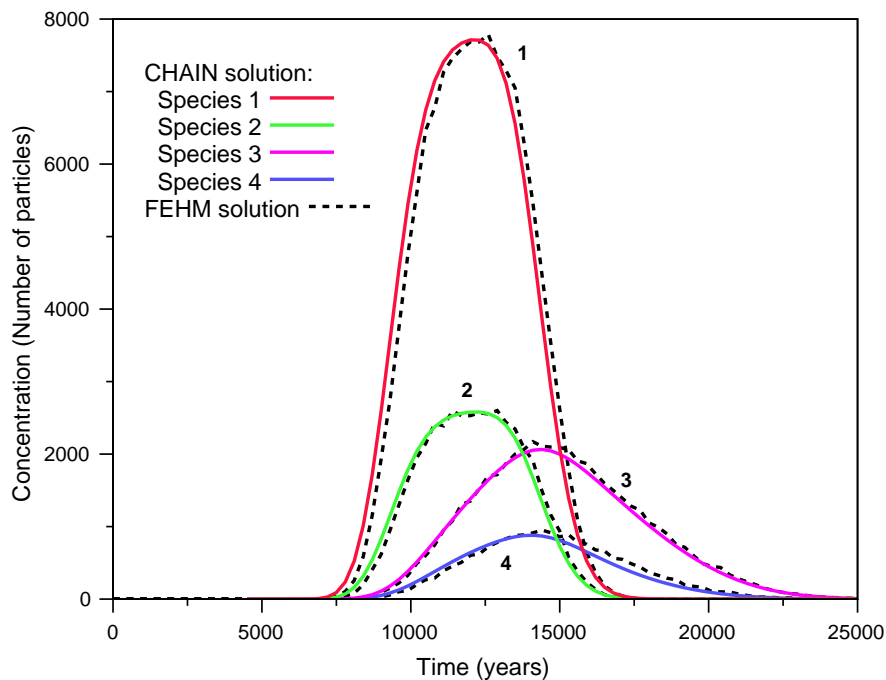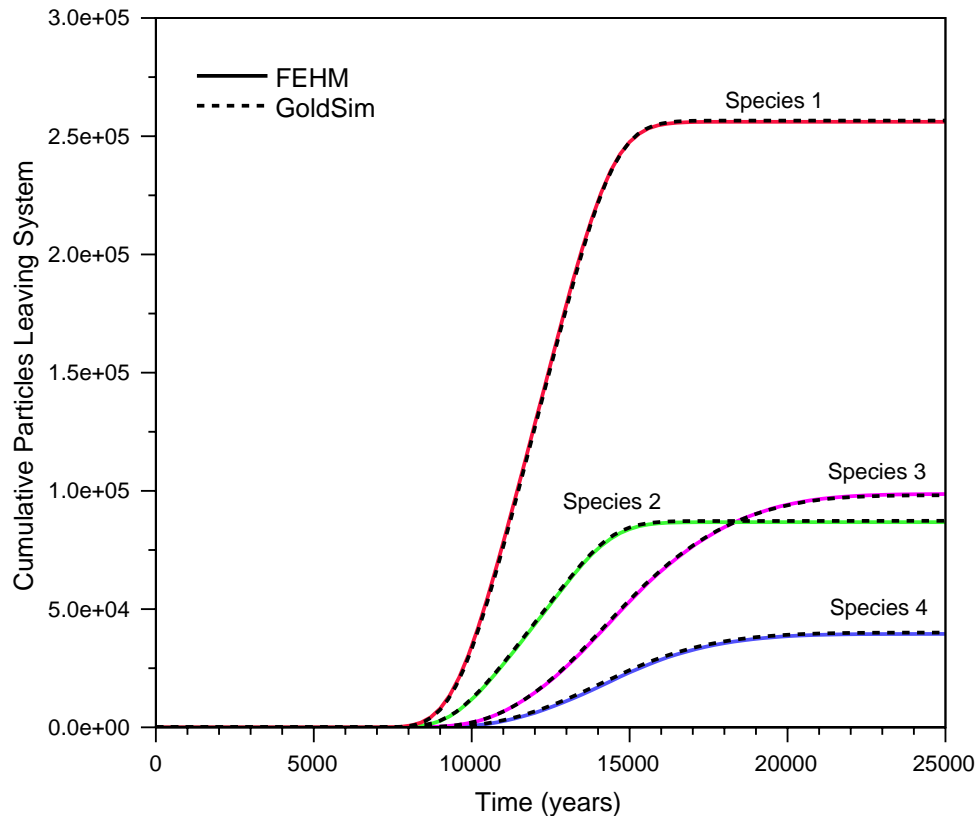cer. Algorithm 1 applies a multi-curve search and interpolation scheme, and also yields excellent agreement for this test problem. Algorithm 2 shows that a simpler nearest neighbor search yields somewhat poorer results. This implies that the nature of the transfer function curves (number of curves and their distribution in the parameter space) has an impact on the closeness of the final result to the actual situation (in this case an analytical solution). This result implies that the spacing and number of transfer function curves is an important factor that must be designed properly to obtain good results.

The second comparison, shown in Figure 62, is for the case of parallel flow in the fracture and matrix, with diffusion but no sorption. Solute mass enters the fracture, and the breakthrough curve corresponds to the combined fracture-matrix breakthrough at the end of the model. The model reproduces the main feature of the breakthrough, namely the dispersed arrival of mass in a time interval between 1 and 100 years. Considering that this is an intermediate case in which the travel times through the fracture and matrix span many orders of magnitude, the agreement with the discrete fracture model is quite good. As discussed above for the first test case, better agreement would be obtained with a distribution of transfer function curves that closely resembles the actual
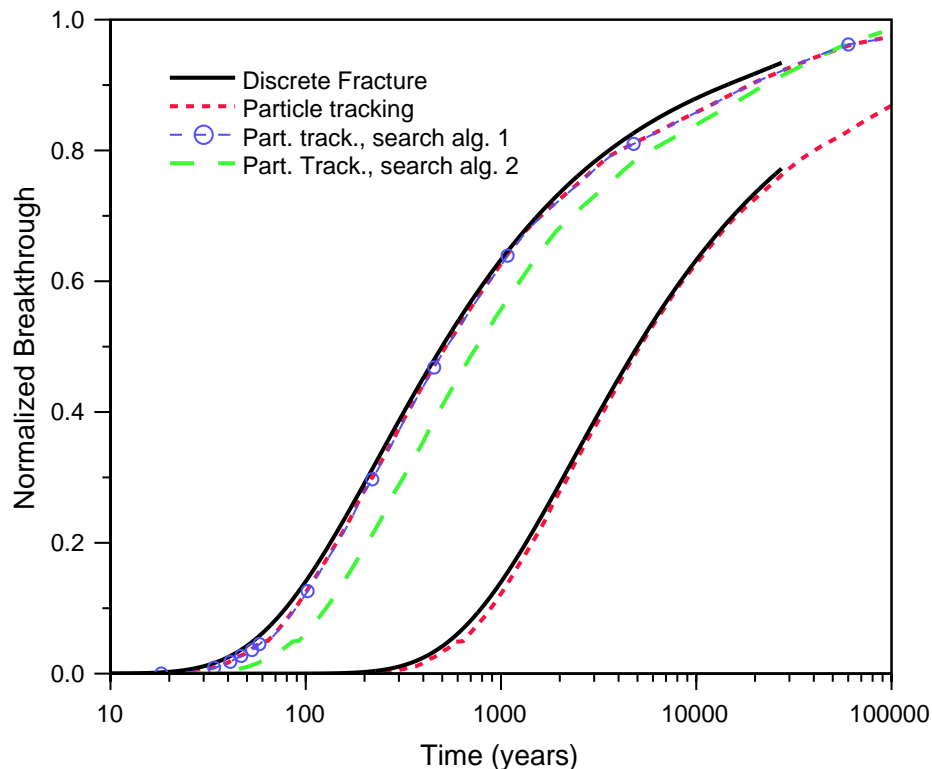
Figure 61. Comparison for the case of flow only in the fracture, with the two-parameter transfer function curves of the Sudicky and Frind (1982) model.

problem. This agreement shows that for the purposes of capturing the matrix diffusion process in a dual permeability model, the results are acceptable, but that the choice of transfer function curves should be main with respect to the problem being solved, so that interpolation does not need to occur over a wide range of parameters.

The final comparison. Figure 63 shows the case of flow transitioning from 90% fracture flow to 60% fracture flow half way down the flow path. The no diffusion case was selected to enable visual testing (by examining the plateau in the breakthrough curve) of the fracture/matrix advective transport part of the model. The first arrival of roughly two thirds of the mass represents the solute that travels in the fracture only. This plateau level is the value that is expected for the no diffusion case. The second arrival of the remaining mass is the portion that moved from fracture to matrix at the transition point, and migrated through the matrix to the outlet. The arrival times of the two breakthroughs can be roughly approximated by the flow rates through the medium. The late arriving mass is dominated by transport through the matrix of 40% of the total flow for one half of the flow distance. The estimated value of about 75 years agrees well with the simulated result. For the fracture arrival, we piece together the two portions of the flow path, compute travel times for each, and sum them. The resulting arrival time is about 0.04 years, also in good agreement with the simulation. As before, even better agreement will be obtained when the transfer
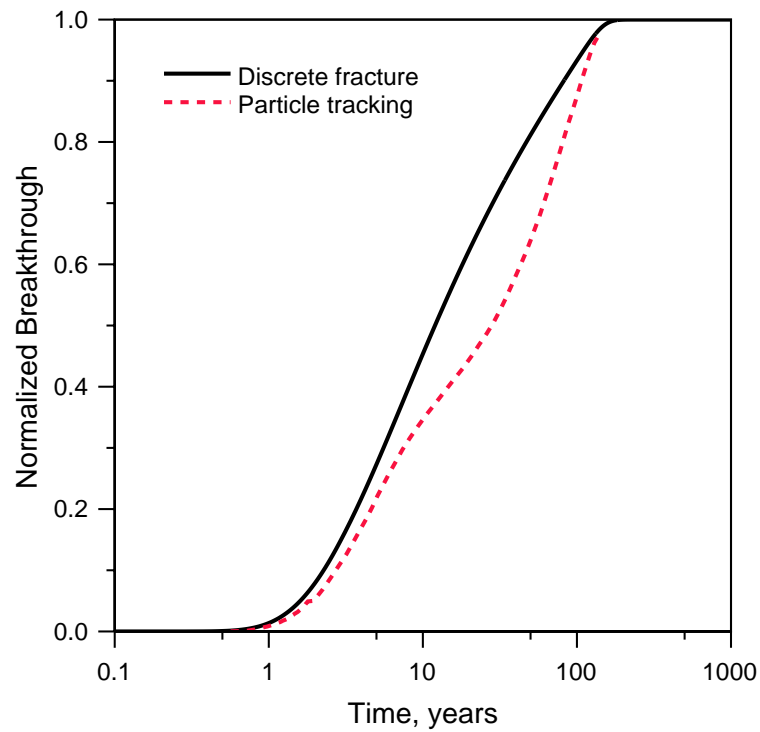
Figure 62. Comparison of parallel flow in the fracture and matrix, with diffusion but no sorption compared to the discrete fracture model.

function curves are selected to be in the range of the simulations, in terms of the parameters of the model. This restriction must be observed when using the model to simulate dual permeability transport.

For the multispecies test a comparison of the number of particles that have left the system and decayed for each species shows the values are within 5%. Particle information from the output file for the final time step is shown in Figure 64.
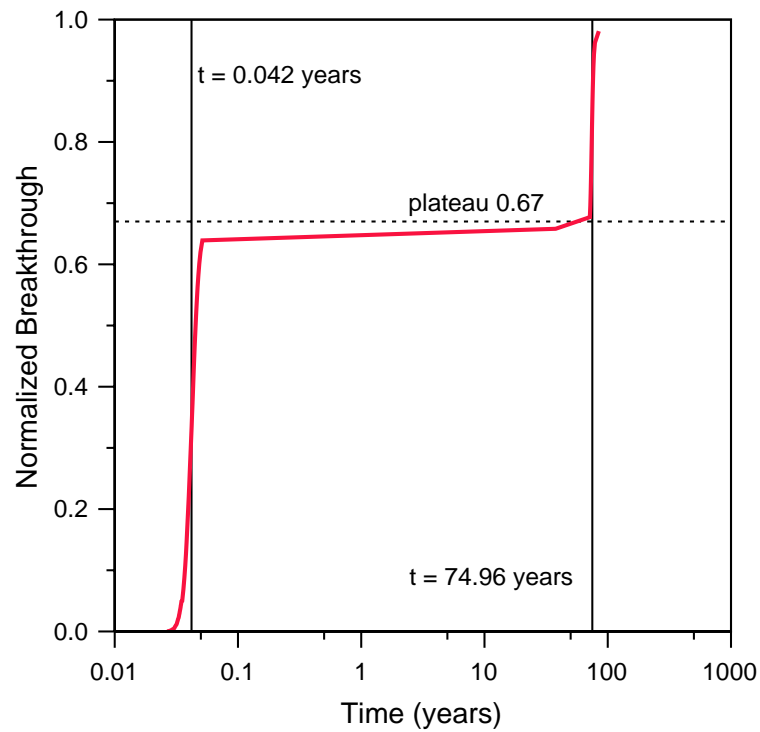
Figure 63. Comparison of flow transitioning from 90% fracture flow to 60% fracture flow half way down the flow path. Theoretical breakthrough times, 0.042 years and 74.96 years, are shown on the plot along with the anticipated plateau of 0.67.

```
Time Step        47


                    Timing Information
         Years              Days          Step Size (Days)
      0.200000E+05      0.730500E+07      0.342479E+05
Heat and Mass Solution Disabled


                 ************************
                  Particle Tracking ==> Species:   1
Number Having Entered System:       18760
Number Currently In System  :        3282
Number Having Left System   :       14919
Number Having Decayed       :         559


  Node    Concentration    # of Particles
     1      0.000000E+00              0
120712     0.000000E+00              0


                 ************************
                  Particle Tracking ==> Species:   2
Number Having Entered System:       18760
Number Currently In System  :        3242
Number Having Left System   :       14991
Number Having Decayed       :         527


  Node    Concentration    # of Particles
     1      0.000000E+00              0
120712     0.000000E+00              0



  simulation ended: days  7.305E+06 timesteps      47



  total N-R iterations =           0
  total solver iterations =          0



  total code time(timesteps) =      59.847363



  ****------------------------------------------------------****
  **** This program for                                     ****
  ****    Finite Element Heat and Mass Transfer in porous media ****
  ****------------------------------------------------------****
  ****              Version : FEHM V2.21sun 03-08-12 QA:QA  ****
  ****              End Date : 08/12/2003                   ****
  ****                  Time : 14:58:18                     ****
  ****------------------------------------------------------****
```

Figure 64. Output from Test of Breakthrough Curve, Dual Permeability Model with Fracture/Matrix Interchange for Multiple Species